Variable Ratio of Permeability to Gating Charge of rBIIA Sodium Channels and Sodium Influx in *Xenopus* Oocytes

Nikolaus G. Greeff and Frank J. P. Kühn
Physiologisches Institut, Universität Zürich-Irchel, CH-8057 Zürich, Switzerland

ABSTRACT Whole-cell gating current recording from rat brain IIA sodium channels in *Xenopus* oocytes was achieved using a high-expression system and a newly developed high-speed two-electrode voltage-clamp. The resulting ionic currents were increased by an order of magnitude. Surprisingly, the measured corresponding gating currents were ~5–10 times larger than expected from ionic permeability. This prompted us to minimize uncertainties about clamp asymmetries and to quantify the ratio of sodium permeability to gating charge, which initially would be expected to be constant for a homogeneous channel population. The systematic study, however, showed a 10- to 20-fold variation of this ratio in different experiments, and even in the same cell during an experiment. The ratio of P_{Na}/Q was found to correlate with substantial changes observed for the sodium reversal potential. The data suggest that a cytoplasmic sodium load in *Xenopus* oocytes or the energy consumption required to regulate the increase in cytoplasmic sodium represents a condition where most of the expressed sodium channels keep their pore closed due to yet unknown mechanisms. In contrast, the movements of the voltage sensors remain undisturbed, producing gating current with normal properties.

INTRODUCTION

Voltage-gated sodium channels are closely related to the other voltage-gated channels that are selective for potassium or calcium, but they excel in having very rapid activation and inactivation kinetics to guarantee the fast impulses of nerve and muscle (Hodgkin and Huxley, 1952; Armstrong, 1981; Hille, 1992; Marban et al., 1998; Armstrong and Hille, 1998). Their function is most commonly studied from ionic currents (I_{Na}) either measured on the single channel or whole-cell level. An additional and more direct insight into the gating machinery of voltage-dependent ion channels is obtained from the gating current (I_g), which was first recorded from sodium channels in the squid giant axon (Armstrong and Bezanilla, 1973; Keynes and Rojas, 1974; for recent reviews see Sigworth, 1994; Bezanilla and Stefani, 1998). I_g is generated by the displacement of charged voltage sensors inside the channel protein, a displacement that couples changes of the transmembranal electric field to the movement of gates that in turn control the permeability of the channel pore. An important finding of the studies by Armstrong and Bezanilla (1973, 1977) was that during inactivation part of the voltage sensors are immobilized and that the time course of recovery from fast inactivation and immobilization is identical. Therefore, gating currents appeared useful for the study of fast inactivation in sodium channels.

In a previous study, using a high-resolution voltage-clamp at the squid giant axon, I_g during the inactivation phase was recorded and correlated with the corresponding I_{Na} (Forster and Greeff, 1990; Greeff and Forster, 1991). These studies strongly suggested the necessity of a voltage sensor for the inactivation process, most likely segment S4 in domain 4 (D4). However, these experiments were limited to wild-type channels in a native preparation that also contained voltage-dependent potassium channels, and it was also assumed that all channels would produce ionic and gating current. It was, therefore, an important step to proceed to heterologous expression systems for designed channels and only a few endogenous voltage-gated channels. So far, evidence for an involvement or coupling of S4D4 in the inactivation process was demonstrated by ionic current experiments at mutant channels (e.g., Chahine et al., 1994; Chen et al., 1996; Ji et al., 1996; Kontis and Goldin, 1997). Gating current experiments from heterologously expressed voltage-gated channels have been exploited in the last years, mostly for potassium channels in *Xenopus* oocytes (e.g., Perozo et al., 1993, 1994; Bezanilla et al., 1994; Aggarwal and MacKinnon, 1996). For sodium channels, the expression was assumed to be too small and the sodium channel kinetics too fast (~5 times faster than in potassium channels) for the measurement of I_g by conventional two-electrode voltage-clamp recording techniques (Ruben et al., 1997). Sophisticated methods like the cut-open oocyte (Stefani et al., 1994; Stefani and Bezanilla, 1998), which has recently been used for $I_{g,Na}$ studies combined with fluorescence (Cha et al., 1999) or the macropatch electrode used for the analysis of gating current fluctuations (Conti and Stühmer, 1989), so far have not permitted the direct quantitative correlation of ionic- and gating-currents for sodium channels. For voltage-gated calcium channels also expressed in transfected cells, such comparisons of gating-charge and ionic current have been successfully performed (Neely et al., 1993; Bangalore et al., 1996; Kamp et al., 1996; Josephson and Varadi, 1996; Jones et al., 1999). In a

Received for publication 28 February 2000 and in final form 15 August 2000.

Address reprint requests to Dr. N. G. Greeff, Institute of Physiology, University of Zürich, Winterthurerstrasse 190, CH-8057 Zürich, Switzerland. Tel.: +41-1-635-5082; Fax: +41-1-635-6814; E-mail: greeff@physiol.unizh.ch.

0006-3495/00/11/2434/20 $2.00

recent study using an optimized two-electrode voltage-clamp we succeeded in recording sodium channel I_g and I_{Na} from S4D4 mutated channels highly expressed in *Xenopus* oocytes, and could directly demonstrate the prominent role of this voltage sensor for inactivation (Kühn and Greeff, 1999).

In the above-mentioned paper and in Greeff et al. (1998) we already reported an obvious mismatch in the size of I_g as compared to I_{Na}. With the aim of clarifying the ratio of gating charge versus conductivity we carried out the present quantitative study measuring both signals simultaneously at the same oocytes. The straightforward two-electrode voltage-clamp technique (TEVC) allowed us to establish fast voltage steps at the whole oocyte, adequate for the recording of I_g (Greeff and Polder, 1998). As detailed now, asymmetry artifacts of the voltage-clamp were minimized and separated from I_g using special pulse protocols. Initially, the ratio of the total gating charge to ionic permeability was expected to be constant if all channels would gate and conduct ions. However, large variations of this ratio were found and always the number of conducting channels seemed to be smaller than the number of gating channels. In the compiled results, we observed a clear correlation with a change of the sodium equilibrium potential most likely caused by a high sodium influx at the channel density used. These data and specific tests strongly suggest that an increase of internal sodium, or rather the energetic stress needed to regulate the cytoplasmic concentration of free sodium, causes a decrease in sodium permeability by lowering the open probability of a fraction of channels with their gating machinery still intact. This finding is of relevance for the supposed ratio of gating charge versus ionic current for rat brain IIA sodium channels expressed in *Xenopus* oocytes, as well as channel modulation. Because the total gating current does not seem to be altered, the improved TEVC technique opens up new possibilities for studying the gating machinery of wild-type and mutant channels. Part of the results of the present study have been published in preliminary abstracts (Greeff et al., 1998; Greeff and Kühn, 2000).

METHODS

Preparation of high-expression RNA

The gene of wild-type rat brain IIA sodium channel α-subunit (rBIIA) used in this study was originally derived from cDNA plasmid pVA2580 (Auld et al., 1988) and transferred into high-expression vector pBSTA (both plasmids kindly provided by Dr. A. Goldin, Irvine, CA; see also Shih et al., 1998). This was performed by subcloning the *Sal*I fragment of pVA2580 containing the open reading frame and 3′ untranslated sequences of the sodium channel gene into the *Bgl*II site of vector pBSTA. For this purpose, both *Sal*I- and *Bgl*II-generated single-stranded ends were partially filled with DNA polymerase I (Klenow fragment) in separate reactions. These reactions filled the first two bases of the 5′ cohesive overhangs left by digestion by *Sal*I and *Bgl*II, respectively, yielding fragments that were no longer self-complementary, but fully compatible with each other for ligation. The correct orientation of the subcloned insert was verified by restriction analysis and DNA sequencing. Plasmid pBSTA contains a T7 RNA polymerase promotor and *Xenopus*-β-globin 5′ and 3′ untranslated sequences. Capped, full-length transcripts were generated from *Sac*II-linearized plasmid DNA using a T7 RNA in vitro transcription kit (Ambion Inc., Austin, TX). Oocytes (stage V–VI) from *Xenopus laevis* (NASCO, Ft. Atkinson, WI) were used. One day before injection of cRNA, the oocytes were defolliculated in a Ca^{2+}-free solution containing 2 mg/ml collagenase (Boehringer, Mannheim, Germany), for 1–2 h at 18°C. Oocytes were microinjected with 20–80 ng of cRNA (50 nl) and maintained at 18 ± 1°C in modified Barth's solution (MBS in mM): 88 NaCl, 2.4 $NaHCO_3$, 1 KCl, 0.82 $MgSO_4$, 0.41 $CaCl_2$, 0.33 $Ca(NO_3)_2$, 10 HEPES-CsOH, pH 7.5, supplemented with 25 U penicillin, 25 μg/ml streptomycin sulfate, and 50 μg/ml gentamycin sulfate.

Electrophysiological recording

Two-electrode voltage-clamp recordings were performed 1–15 days after cRNA-injection with a TEC-05 (npi-electronics, Tamm, Germany) that had been modified in collaboration with R. H. Polder from npi-electronics for optimal series resistance (R_s) compensation and fast charging of the membrane capacitance (Greeff and Polder, 1998). Intracellular electrodes contained an agarose cushion (Schreibmayer et al., 1994), were filled with 3 M KCl, and had resistances between 100 and 200 kΩ. Macroscopic ionic- and gating-current signals were recorded using a PDP-11/73 (Digital Equipment Corp., Maynard, MA) controlled 16-bit A/D and 12-bit D/A interface (CED, Cambridge, UK). The oocytes were clamped at a holding potential of −100 mV for at least 5 min to ensure recovery of slow inactivation before recording started.

R_s compensation was adjusted for critical settling of the capacitance transients within 100–200 μs (Greeff et al., 1982). The charging of the membrane was then speeded up optimally without subsequent ringing, which would distort the gating currents. At the same time a reduction of voltage errors due to large ionic currents was achieved. In our study the macroscopic ionic currents were large and prone to R_s errors in two respects, as seen in the Results. First, at all voltages, for the capacitance as well as for the ionic current, a voltage error occurs, being the product of uncompensated R_s and current size. Second, in the very nonlinear voltage range of the sodium activation curve around −40 mV, such voltage errors distort the normal activation more pronouncedly than in the more linear region above 0 mV. This behavior is especially prominent for membrane regions that are not well space-clamped. In our experiments we improved our technique in this respect. In the early phase the oocytes were pressed against the chamber floor, which could lead to a bottom region of the membrane with a different series resistance, resulting in space-clamp errors. In the later experiments the cells were slightly lifted, which seemed to create better space-clamp conditions. Compare the "escaping" sodium current traces (see Figs. 3 and 5) and the better-recorded *I*/*V* curves (see Fig. 6). A further relevant point was that we—in contrast to the situation assumed in the methodical study by Baumgartner et al. (1999)—placed the current electrode tip deep into the cell to achieve a more homogeneous spatial charging of the membrane. As we could check on the recorded capacitance transient, an eccentric position of the electrode showed up as a slow tail that could not be compensated critically, an observation known to us from squid axon experiments. For the calculation of R_s and its uncompensated part, dummy studies were performed. Reliably, we could estimate the uncompensated part from the speed of the critically compensated transient. In contrast to the situation in the cell, this could be confirmed in the dummy by comparing the voltage levels due to DC-current at the point of current injection and between the series resistance and the membrane resistance in parallel to the capacitance. Corresponding calculations for the experimentally observed ionic currents will be given in the Results. In order to know the clamping speed, we routinely stored the capacitance transients.

No analogous subtraction was used because the 16-bit ADC had a sufficiently fine resolution for digital subtraction of the large linear tran-

sient and leak currents by scaled averages from pulses below −100 mV (for basic protocols see Bekkers et al., 1984). Reduction of the remaining asymmetry was achieved by finding a compromise between clamping speed and asymmetry, i.e., low-pass-filtering the command signal at 5 kHz (8-pole Bessel filter, Frequency Devices, Haverhill, MA, U.S.A.). Recorded signals were low-pass filtered at 5 kHz (8-pole Bessel filter, Frequency Devices) and sampled at 10 or 20 kHz. Data analysis was performed on the PDP-11/73; permeability calculations were done in MathCad (MathSoft, Inc., Cambridge, MA). The experiments were carried out in MBS solution at different bath temperatures (8–15 ± 1°C) and in some cases a fraction of Na^+ was replaced by an equimolar amount of choline, as indicated in the experiments. For the recording of gating currents, either 2 μM tetrodotoxin (TTX; RBI Research Biochemicals International, Natick, MA, U.S.A.) was added or recordings were performed at the sodium reversal potential as described in the text.

Permeability calculations

During the course of the experiments for this study the problem arose that sodium ionic currents obtained under different conditions, such as varying external and internal sodium concentrations, had to be compared. Furthermore, for an estimate of the number of conducting channels the published figures for single channel currents had to be used that had been obtained at conditions favorable for single channel recording, i.e., in a voltage region of −60 to −10 mV. In order to avoid the above-mentioned distortions due to R_s errors in the nonlinear voltage region, we adopted the method of obtaining the conductance around the sodium reversal potential E_{Na}. For the comparison of such different experimental data we transformed the current and conductance G_{Na} to permeability P_{Na}. This, as discussed later on, despite not being the perfect method, is a very good method for an estimate of the amount of open channels independent of both the sodium concentration and the voltage range of the test-pulse.

According to the Goldman-Hodgkin-Katz-theory, the current I_{Na} that flows through open channels with a given P_{Na} depends on the pulse potential V and the sodium concentrations on either side of the membrane, $[Na^+]_i$ and $[Na^+]_e$, as follows (see, e.g., Hille, 1992, Eq. 13.5):

$$I_{Na}(V) = P_{Na} \cdot z^2 \cdot V \cdot K \cdot F \cdot \frac{[Na^+]_i - [Na^+]_e \cdot \exp(-z \cdot V \cdot K)}{1 - \exp(-z \cdot V \cdot K)} \quad (1)$$

where K equals F/(R*T) with their usual meanings, and z is the valence. In our experiments the internal sodium concentration was unknown, but was derived from the experimentally observed reversal potential assumed to correspond to the sodium equilibrium potential E_{Na} using the Nernst equation. Substituting $[Na^+]_i = [Na^+]_e/\exp(E_{Na} * K)$ and setting $z = 1$ in Eq. 1 one obtains:

$$I_{Na}(V) = P_{Na} \cdot V \cdot K \cdot F \cdot [Na^+]_e \cdot \frac{\exp(-E_{Na} \cdot K) - \exp(-V \cdot K)}{1 - \exp(-V \cdot K)} \quad (2)$$

Often the ionic currents are expressed as current per area of membrane, and then the permeability has the dimension of distance per time. In our approach we preferred to compare the absolute currents of whole oocytes with currents through single channels and expressed the permeability by the volume that is cleared per time. A typical figure for the single channel current from cell attached recordings at an oocyte in ND96 bath containing 96 mM sodium is reported to be 0.9 pA at $V = -30$ mV at room temperature (same sodium channel clone rBIIA as in our study; Goldin, 1991). Assuming a typical E_{Na} of +51 mV corresponding to a reasonable figure of 12 mM for $[Na^+]_i$, we calculated the single channel permeability P_{Na} by solving Eq. 2 and obtained P_{Na} equal to $5.8 \cdot 10^{-5}$ pl/s. This figure as also the figure for the more familiar conductance $\gamma = i_{Na}/(V - E_{Na})$ equal to 11 pS will be used for the estimate of the number of conducting channels in the Discussion.

It will be further useful to consider the first derivative dI_{Na}/dV of Eq. 2 to obtain the permeability from the conductance around E_{Na}, which is measured reliably also at high channel expression, because around E_{Na} the ionic currents remain small and are only subject to linear R_s errors (discussed in the Results). From Eq. 2 follows by differentiation:

$$\frac{dI_{Na}}{dV}(V) = P_{Na} \cdot K \cdot F \cdot [Na]_e \cdot (T1 + T2 + T3) \quad (3a)$$

where

$$T1 = \frac{e^{-E_{Na} \cdot K} - e^{-V \cdot K}}{1 - e^{-V \cdot K}} \quad (3b)$$

$$T2 = \frac{K \cdot V \cdot e^{-V \cdot K}}{1 - e^{-V \cdot K}} \quad (3c)$$

$$T3 = \frac{K \cdot V \cdot [e^{-K \cdot (V + E_{Na})} - e^{-2 \cdot V \cdot K}]}{[1 - e^{-V \cdot K}]^2} \quad (3d)$$

The relevance of these computations is shown graphically in Fig. 1 based on the single channel data from above: single channel current i_{Na} of 0.9 pA at $V = -30$ mV at room temperature, cell-attached recording from an oocyte with sodium concentrations $[Na^+]_e$ of 96 mM (Goldin, 1991), and a typical $[Na^+]_i$ of 12 mM.

The cord conductance $i_{Na}/(V - E_{Na})$ would give $\gamma = 11$ pS (straight line s(c, −30)). The ionic current through an open channel according to Eq. 2 depends on voltage and the asymmetrical sodium concentrations. Therefore, the slope conductance $dI(V)/dV$ varies, which is visible in Fig. 1, *A* and *B*. Around the equilibrium potential E_{Na} of +51 mV the slope $dI(V)/dV$ equals 6.55 pS (tangent s(E_{Na}), in 1 *A*; level in 1 *B*), while it would be ~16 pS at −30 mV, which is between 22 pS at very negative and 2.8 at very positive voltages (current determined by either external or internal concentration only). The slope conductance dI/dV at E_{Na} (the observed E_{rev}) was experimentally obtained, and from its value together with $V = E_{Na}$ one obtains the figure for P_{Na} using Eq. 3, which simplifies because $T1$ and $T3$ become zero:

$$P_{Na} = \left[\frac{dI}{dV}\right]_{E_{Na}} \cdot \frac{e^{E_{Na} \cdot K} - 1}{E_{Na} \cdot K^2 \cdot F \cdot [Na]_e} \quad (4)$$

The permeability P_{Na} does not depend on the sodium concentrations of the solutions adjacent to the conducting channels, but indicates how much volume is cleared per time, while the current and the conductance also depend on the ion content of this volume. Therefore, experimental data obtained with varying external or internal concentrations can directly be compared via P_{Na}.

To test the usefulness of P_{Na}, it will be necessary to fit an equation to I_{Na} versus V when a whole family of sodium currents for different voltages is obtained. Simply fitting a Boltzmann curve to G_{Na} versus V would not fit well, and especially would not account for different ionic concentrations. Therefore, we decided to combine the conversion of current to permeability and the Boltzmann relation. For this purpose Eq. 2, which reflects the change of the current at different voltages and sodium concentrations for a constant permeability P_{Na} corresponding to a constant number of open channels, is now multiplied with the Boltzmann term raised to the third power. In that way, the voltage-dependence of open probability is incorporated similar to the Hodgkin and Huxley formalism (Hodgkin and Huxley, 1952), but for the peak sodium currents uncorrected for inactiva-

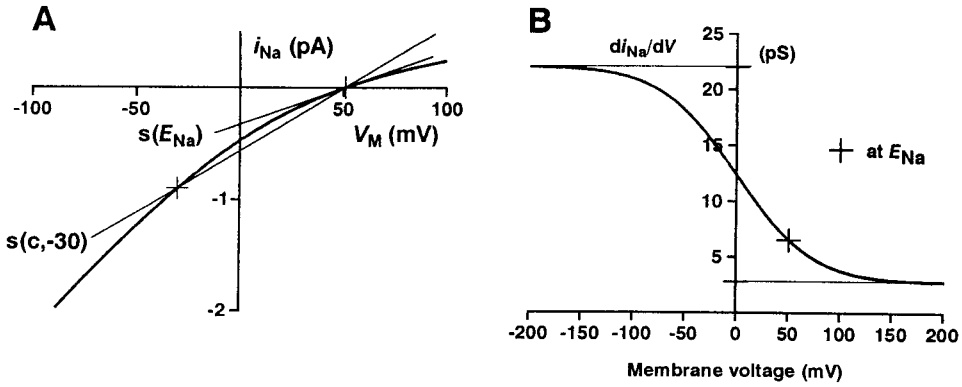

FIGURE 1 Single channel conductance i_{Na} (*A*) and its derivative di_{Na}/dV (*B*) versus pulse potential as calculated from Eqs. 2 and 3 assuming a constant permeability for the channel of $5.8 \cdot 10^{-5}$ pl/s and asymmetrical, typical $[Na^+]_e/[Na^+]_i$ of 96/12 mM corresponding to E_{Na} of +51 mV. The different figures for the cord conductance s(c, −30), the slope conductance at various voltages, and especially s(E_{Na}) at E_{Na}, are discussed in the text.

tion, as it is often used:

$$I_{Na}(V) = \frac{P_{Na} \cdot V \cdot K \cdot F \cdot [Na]_e}{(1 + \exp((V' - V)/A))^3} \cdot \frac{\exp(-E_{Na} \cdot K) - \exp(-V \cdot K)}{1 - \exp(-z \cdot V \cdot K)} \quad (5)$$

where V' is the half-activation voltage and A the slope factor.

RESULTS

Expected size and identification of sodium channel gating current: increase of channel expression

The known properties of ionic- and gating-current from sodium channels of squid and other preparations are used here for a first estimate of the expected size of the gating current (I_g) (Fig. 2). During activation, charged voltage sensors (S4 segments) move along the electric field in the channel protein and, by coupling to a gating structure, control the opening of the pore (Stühmer et al., 1989; Yang and Horn, 1995; Yang et al., 1996). The individual S4 movements are assumed to occur between energetically favorable states (Fig. 2 *B*). According to the present understanding a channel has to go through a number of closed states (C_0, C_1, C_5), separated by charge-producing transitions before the channel pore is open for sodium ions to pass (state O in state diagram of Fig. 2 *B*). Voltage-dependent transitions produce specific amounts of charge displacement (q_{0-5}), around 1 electron charge (e_o), that cause single channel gating current shots (i_g in Fig. 2 *C*) which, however, are far too small to be detected individually. In the open state, a single channel ionic current (i_{Na}) of ~1 pA flows (equivalent to ~5000 sodium ions/ms), until the inactivation gate closes the channel. The sum of these stochastic single channel signals is measured as the total macroscopic ionic current (I_{Na}) and gating current (I_g) of all channels in the cell membrane. I_{Na} shows an activation and an inactivation phase, I_g occurs mainly during the activation phase (Fig. 2 *C*). Each channel produces a constant amount of gating charge per channel ($\Sigma q = q_0 + q_1 + \ldots q_5$) the size of which is still a point at issue, estimations ranging from 4 to 6 (Hille, 1992; Sigg and Bezanilla, 1997) to 12 e_o (Hirschberg et al., 1995). A mean value of 8 e_o will be assumed in the Discussion. A further phenomenon specific for sodium channels is gating charge immobilization. In a two-pulse protocol with a short interpulse interval at holding potential, the second pulse will elicit no transient I_{Na}, but still a fraction of gating current ($I_{g,\,n}$) that is assumed to occur from channels switching quickly between inactivated states (Armstrong and Bezanilla, 1977; Bekkers et al., 1990) or, with respect to molecular structure, only part of the voltage sensors, are able to return while the pore is still closed by the inactivation h-gate. Part of the structure responsible for inactivation and immobilization is most likely the cytoplasmic loop connecting domains D3 and D4 (Vassilev et al., 1988; Stühmer et al., 1989; Patton et al., 1992). Recent work suggests that the S4 voltage sensors in D1 and D2 are free to move during inactivation, while those in D3 and D4 are immobilized (Cha et al., 1999) and our own results suggest that it is S4D4 that controls the movement of the loop (Greeff and Forster, 1991; Kühn and Greeff, 1999).

Starting the experiments in search of gating currents, initially a rough comparison of peak amplitudes of the macroscopic currents to be expected from N channels with single channel current i_{Na} was made. The ionic current is expressed as

$$I_{Na,peak} = N \cdot i_{Na} \cdot p^o \cdot F^a \quad (6)$$

and p^o is the probability of a channel to be open at peak time; p^o is ~0.5 for voltages of 0 mV and above as deter-

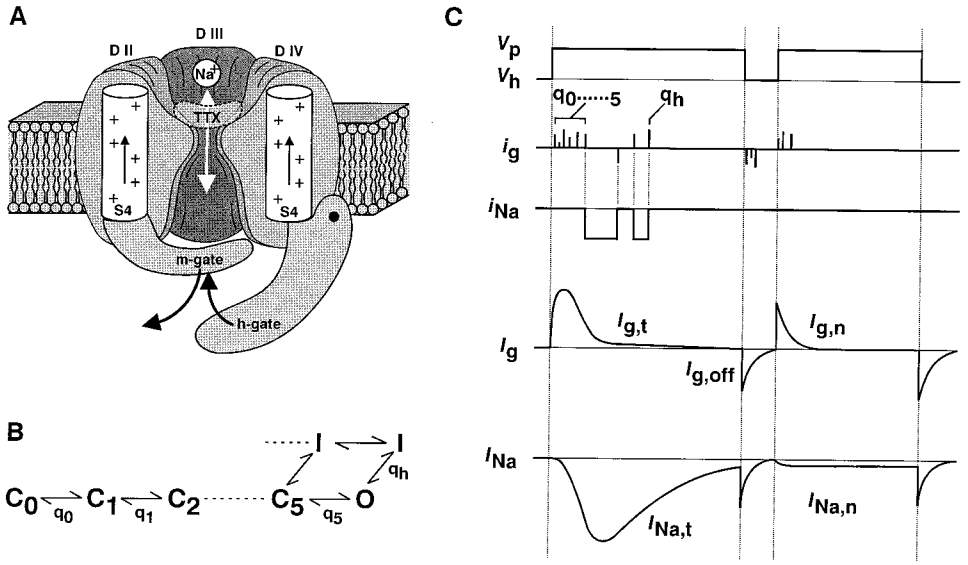

FIGURE 2 Schematic working model illustrating the essential features of sodium channel ionic and gating currents. (*A*) Cross-section of the α-subunit of the sodium channel protein, with its four domains D I–D IV (D I is omitted to lay open the pore); each domain has 6 putative membrane-spanning segments S1–S6 (not detailed). The S4 segments of D I–D III control the m-gates (shown for D II), whereas segment S4 of D IV is coupled to the h-gate. The molecular mechanisms of this coupling are treated elsewhere (Kühn and Greeff, 1999). The highly specific, external sodium channel blocker tetrodotoxin (TTX) is depicted in its assumed functional position. The outward movement of the S4 voltage sensors caused by depolarization is indicated by arrows. (*B*) State diagram assuming 6 closed states (C_0 to C_5) with quantal displacement charges of activation (q_0 to q_5), the open state (O), and several inactivated states (I); q_h, quantal displacement charge O to I. (*C*) Signals during a test pulse that activates and inactivates the sodium channels, a short gap at holding potential, and a second pulse occurring when the channels are still inactivated. Abbreviations: V_p, command voltage pulses; V_h, holding potential; q_{0-5}, q_h, quantal gating charges of the S4 voltage sensors that cause the single channel gating current shots (i_g) due to the movements of the voltage sensors for the activation and inactivation gates, respectively; I_g, macroscopic gating current of the total number of channels; $I_{g,n}$, nonimmobilized fraction of I_g; i_{Na}, single channel sodium ionic current; I_{Na}, macroscopic sodium ionic current; $I_{Na,n}$, remaining, noninactivating fraction of sodium current after inactivating prepulse.

mined directly by the method of nonstationary fluctuation analysis at the node of Ranvier (Sigworth, 1980), in squid (Bekkers et al., 1986), and neuroblastoma cells (Bulatko and Greeff, 1995). F^a equals 1 if all channels that produce gating current are a homogenous population with the same normal probability p^o. This is assumed at first, but if some channels keep their pore closed for some reason or bypass the open state, F^a will be between 0 and 1; this would correspond, e.g., to modulated channels (Bulatko and Greeff, 1995) or to channels with their pores closed by TTX. The gating charge of N channels, each contributing Σq, equals:

$$Q_g = N \cdot \Sigma q \tag{7}$$

I_g occurs mostly during the time t_p to peak of I_{Na}. We found that I_g was of nearly triangular shape, especially when filtered, and then the following approximation for its peak is useful:

$$I_{g,peak} = \frac{N \cdot \Sigma q \cdot 2}{t_p} \tag{8}$$

Injection of large amounts (30–80 ng) of cRNA from conventional vectors yielded an average maximal inward current $I_{Na,\,peak}$ at voltages ~ -10 mV of ~ -5 μA (unpublished data). Taking i_{Na} as 0.9 pA (Goldin, 1991) and p^o as 0.5, we calculate from Eq. 6 a total channel number N of 11×10^6 per oocyte. Assuming all these channels to be fully functional ($F^a = 1$), $t_p = 1$ ms (for the applied test-voltage) and $\Sigma q = 8$ e_o, one would expect from Eq. 8 an $I_{g,peak}$ of $\sim$0.03, μA which gives a ratio for $I_{Na,peak}/I_{g,peak}$ of $\sim$160:1. This fits with other estimations around 100:1 for mammalian sodium channels expressed in *Xenopus* oocytes (unpublished, from personal discussions). Such a small gating current would be hardly detected in the baseline noise of a two-electrode voltage-clamp. Therefore, our primary aim was to increase the density of channels by applying a high-expression vector designed for *Xenopus* oocytes that had already been successfully used for potassium channels (Perozo et al., 1993); the cRNA contains code-flanking β-globin, a 3′-end poly-A tail and 5′-end cap. With this technique we could increase $I_{Na,peak}$ by a factor $\sim$10 with maximal amplitudes of between -50 and -150 μA (typical recordings Fig. 5 *A*), and we expected for $I_{g,peak}$ 0.3–0.9 μA.

Very fast clamp and short asymmetry: unexpectedly large putative gating current

Because sodium gating currents were expected to be very fast, we initially tried to speed up the clamp as fast as

possible and would even accept some asymmetry artifacts due to some nonlinearity in recording and subtraction of the capacitance transients. It was possible to speed up the charging of the whole oocyte membrane to a settling time of the capacitance transient in ~60 μs (Fig. 3); this, however, caused transients I_c with amplitudes of 500–600 μA. These fast and large transients obtained for the forward pulses were not subtracted well using subtraction pulses between −100 and −150 mV. The resulting asymmetry artifacts gave erratic zigzag lines of ~10–20 μA (Fig. 3 *D*). This contamination might obscure the gating current with respect to amplitude, but since it lasts only 60 μs it could be blanked, still leaving time to display the slower gating current (demonstrated in Fig. 3, *D* and *E*; expanded time base). As a result, the putative gating current can be clearly identified even in the nonexpanded traces of Fig. 3 *A*. It showed typical gating current properties: always flowing outward in contrast to the ionic current and occurring in <1 ms before the peak of the ionic current. The size of several μA, however, was unexpectedly large, being nearly of equal amplitude as the ionic currents, so we had serious doubts about its origin.

These experiments also demonstrated the performance of our TEVC with respect to speed and linearity. It is possible to charge the large membrane capacitance of 200–280 nF within <100 μs. The integrated transients represent the time course of the voltage at the very membrane as it is charged to the command voltage (Fig. 3 *C*). From their 10–90% rise-time of 23 μs the time constant is calculated as 23/2.3 = 10 μs (Horowitz and Hill, 1980). This allows us to

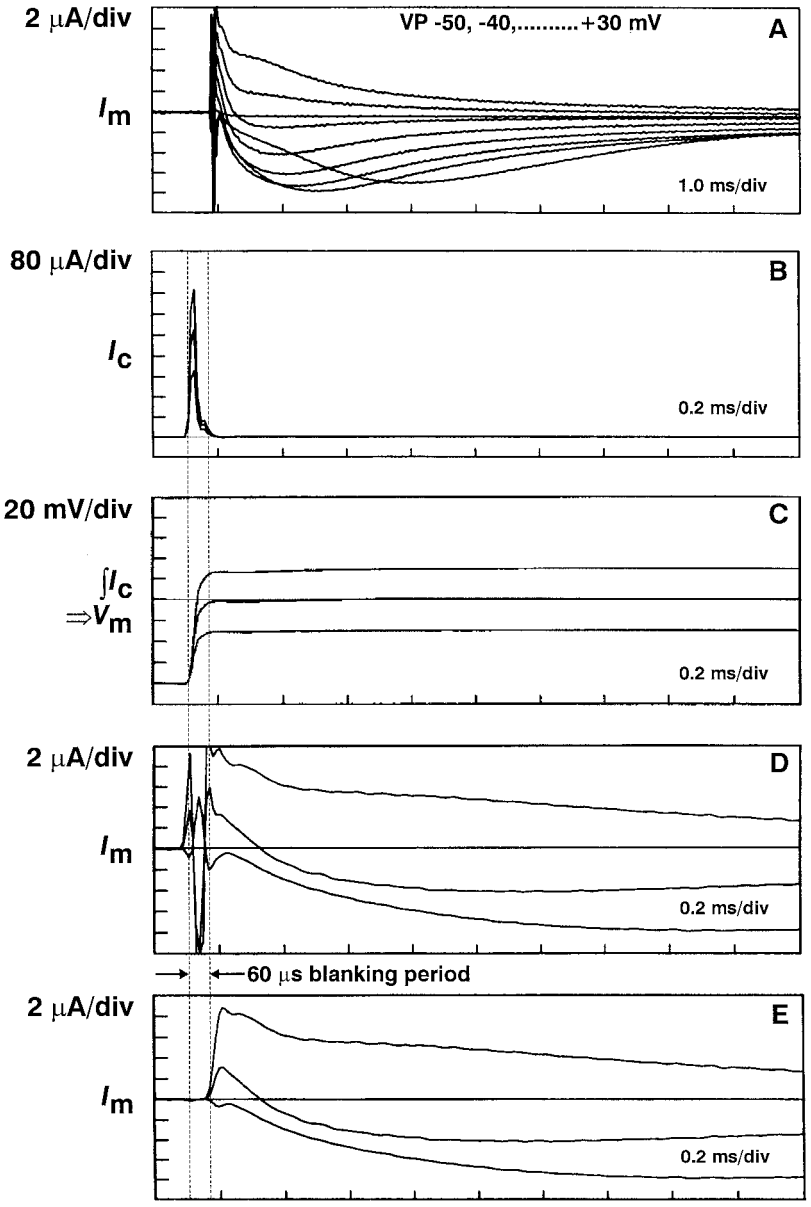

FIGURE 3 Recordings with a voltage-clamp tuned for speed and critical R_s compensation. (*A*) Testpulses from −50 to +30 mV in steps of 10 mV; pulses for subtraction of linear components were between −100 and −150 mV; note the escaping trace at −40 mV. (*B–E*) signals of −30, 0, +30 mV on expanded timescale; the vertical dotted lines indicate the settling time of the membrane voltage. (*B*) Capacitance transients (I_c) and (*C*) their integral, which reflects the time course of charging the cell membrane (V_m) to the command voltage. (*D*) Signal traces of membrane current $I_m = I_{Na} + I_g +$ contamination show the zigzag due to non-ideal subtraction of the capacitance transients of forward test pulse and linear subtraction pulse. The zigzag is followed by putative outward gating currents and ionic sodium currents, which change polarity when V_p crosses the sodium reversal potential. (*E*) Same as *D* but data points during nonlinear subtraction of transients were blanked. Experiment T18M.I; temperature 8°C.

obtain an estimate of the remaining series resistance, which was not compensated as $R_{s,r} = \tau/C_m = 10\ \mu s/0.25\ \mu F$ equal to 40 Ω. As detailed above, this method to estimate R_s was verified on a dummy and should also be representative for the I_{Na} traces. However, the observed escaping trace at −40 mV would then only suffer from a voltage error of 8 μA times 40 Ω, equal to 0.32 mV, which would not explain this distortion. At this early stage of the experiments we were not so conscious about electrode positioning and contact area of the oocyte with the bottom of the chamber. We now assume that the charging of the membrane was not perfectly homogeneous with respect to space-clamp, which allows small membrane areas to produce uncontrolled ionic-current (see Methods for improvement). More important was a reduction of the artifact due to nonlinear subtraction of the huge transients. From studies on dummy membranes we noticed that this asymmetry occurred mainly during the fast changes (large time derivative) in the capacitance transient. Therefore, our next strategy was to slow the clamp such that it still would be adequate for gating-current recording.

Slightly slower and improved voltage-clamp with little asymmetry confirms large gating current

To decide whether the observed asymmetrical charge displacement had its origin in clamp artifacts or actually reflects charge movement in sodium channels, we reduced the clamp asymmetries by compromising on the speed and applied special protocols for the separation of the two possible sources for asymmetry current. Improvements on the technical side were as follows: 1) slowing the command pulse from the D/A converter by feeding it through an 8-pole Bessel low-pass filter set at 5 or 3 kHz; 2) checking all gain stages in the voltage-clamp to avoid any saturation of an amplifier with respect to gain and slew rate; 3) using low-resistance electrodes of 100–200 kΩ. These means resulted in a capacitance transient of a much smaller amplitude and roughly triangular shape, as seen in noninjected control oocytes (Fig. 4, *A* and *B*). The 10–90% rise-time was ~180 μs, corresponding to a time constant of 180/2.3 = 80 μs when the command pulse was rounded at 5 kHz, and the resulting signal filtered again at 5 kHz for reduction of noise before A/D conversion. In an analogy to the above calculation, a remaining R_s of some 300 Ω would be obtained. This, however, is an upper limit as checked on a dummy because the rounding of the command pulse and low-pass filtering of the recorded transient mask the effective R_s compensation. Escaping ionic current traces still were sometimes observed for large currents (40 μA in Fig. 5 *A*), but often with well-placed electrodes the *I*/*V* curves were only a little distorted (compare Fig. 6). The nonlinearity in the subtraction of the capacitance transient was greatly reduced. A full transient of 200 μA amplitude resulted in an asymmetry of <1 μA of various shape. Typically, we obtained a fast downward spike during the rising phase of the ON-transient (Fig. 4 *A*), but asymmetries lasting slightly longer than the transient and in the direction of I_g could also be seen (Fig. 4 *B*). Analog subtraction of the transient before digitization did not improve the transient cancellation and was not necessary, because our 16-bit ADC had enough resolution to avoid digitization noise in the records. We regarded this amount of clamp asymmetry as acceptable in view of the large gating current, but carried out further test protocols to distinguish real gating current from the overlapping asymmetry in channel-expressing cells.

The strongest proof for the identification of the sodium gating current was obtained by checking for the typical partial immobilization of sodium gating charge as detailed schematically above (Fig. 2 with references). As the experiment in Fig. 4, *C–F* shows, a test pulse to −20 mV did elicit a large ionic current with a clear activation and inactivation phase. The same pulse applied after an inactivating prepulse to +20 mV for 20 ms elicits no or few ionic currents (depending on the duration of recovery during the gap at holding potential) and only reopens a variable amount of noninactivating sodium channels (Fig. 4 *C*). Gating currents were recorded after the addition of 2 μM TTX to the bath with test pulses ranging from −80 mV to +80 mV in steps of 20 mV, first in the absence of an inactivating prepulse (Fig. 4 *D*). The same pulses applied after an inactivating prepulse demonstrated a reduction of the ON-gating currents by ~50% (Fig. 4 *E*). Typically, this nonimmobilized gating current $I_{g,n}$ displays a faster time course compared to the total $I_{g,t}$. The clamp asymmetry of several μA was relatively large in this particular experiment (also chosen to better demonstrate the procedure) and it clearly did not change when a prepulse was applied (compare Fig. 4, *D* and *E*). This is expected for a clamp asymmetry, as can also be seen for the control cell in Fig. 4 *B*. The immobilization of our gating current signal in contrast to clamp asymmetry is evident after subtraction of the traces without and with a prepulse (Fig. 4 *F*).

We were then in a position to embark on a detailed quantitative comparison of sodium channel gating- and ionic-current and to check whether their ratio would be a constant. For this purpose we systematically measured I_g and I_{Na} from the same oocytes. Fig. 5 *A* shows a family of ionic and gating currents for a series of test-pulses ranging from −40 to +60 mV in steps of 10 mV obtained under optimized conditions at 8°C, where the fast sodium channel currents are slow compared to the capacitance transient. Despite more cautious R_s treatment and electrode positioning, for the large ionic currents of some 30 μA proper control of space-clamping was still a problem, as the escaping trace at −40 mV shows. However, as can be clearly seen, the ionic current changes its polarity from inward to outward when crossing the equilibrium potential for sodium at ~+23 mV, in this case. In contrast, the gating current that precedes the ionic current is always flowing along the polarity of the test-pulse. We took advantage of this by

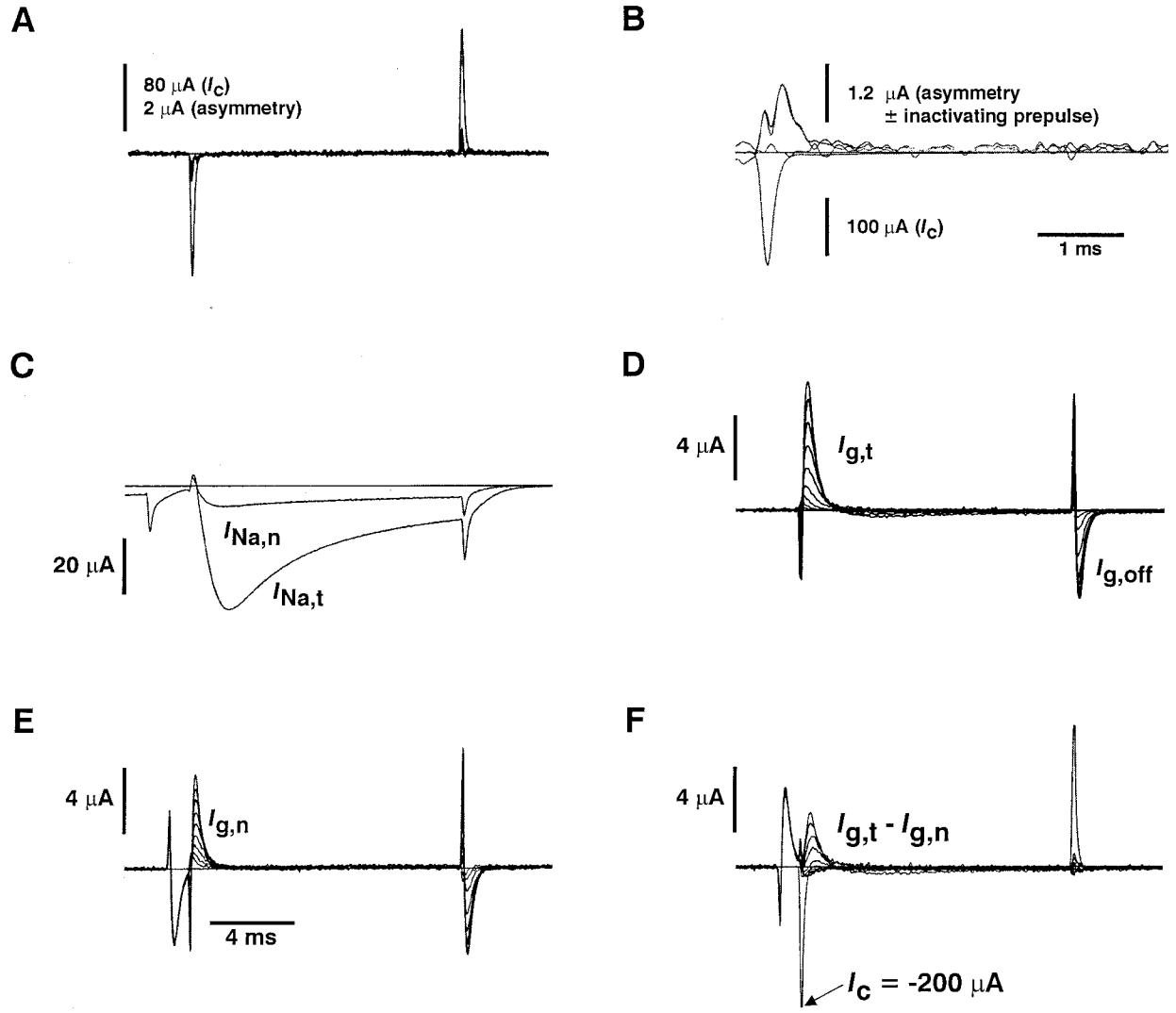

FIGURE 4 Sodium ionic and gating currents versus clamp-asymmetries with and without inactivating prepulse from noninjected control cells (*A*, *B*) and cRNA-injected cells (*C–F*). (*A*) Difference of capacitance transients for test pulses of 13 ms duration to −40 mV up to +40 mV in steps of 10 mV from a holding potential (V_h) of −100 mV; subtraction pulse between −120 mV and −150 mV with its transient (I_c) shown scaled to the +40 mV testpulse: full transient of 150 μA, corresponding difference 0.88 μA, duration as full transient, equal in ON and OFF. (*B*) Another example with an outward asymmetry that in addition lasts longer than the full transient, amplitudes 196 and 1.4 μA; the asymmetry is shown for the same test pulse with and without inactivating prepulse. (*C*) Recordings of I_{Na} in MBS solution with and without inactivating prepulse to +20 mV for 20 ms; interval of 2 ms at V_h; test pulse to −20 mV for 13 ms. (*D*) Gating current with medium-sized contamination as in control cell of *A*, recorded in MBS containing 2 μM TTX; no inactivating prepulse; series of test pulses from −80 mV to +80 mV in steps of 20 mV, pulse duration 13 ms. (*E*) Same as *D* but with 20 ms inactivating prepulse to 0 mV; interval at V_h 1 ms; $I_{g,off}$ of inactivating prepulse included in time window. (*F*) Difference resulting from digital subtraction of recordings in *E* from those in *D*; I_c capacitance transient for pulse to +80 mV. Timescale: 4 ms bar as in *E* for all panels except for *B* 1 ms. Recordings taken at a holding potential V_h of −100 mV; temperature 8°C.

stepping in small increments across the reversal potential (Fig. 5 *B*). Then, the ionic currents are small despite the large number of activated channels and only subject to linear R_s errors in this part of the *I*/*V*-curve, and at exactly E_{Na} no net ionic current flows, leaving an almost pure gating-current signal. From these recordings we obtained at the same time the total gating current $I_{g,t}$ and the sodium conductance dI_{Na}/dV at E_{Na}. Initially, we considered applying partial TTX block of the sodium channels to reduce the ionic current and thus avoid R_s errors. The partial reduction by TTX, however, is not well defined due to use-dependent block (Patton and Goldin, 1991; Conti et al., 1996). Furthermore, the simultaneous recording of I_{Na} and $I_{g,t}$ ensured that no channel loss could occur while waiting for the TTX to block. To demonstrate the absence of sodium ionic contamination we did control experiments where we compared the gating current at E_{Na} before applying TTX and quickly after adding it to the bath (see Fig. 10 *A*, *inset*).

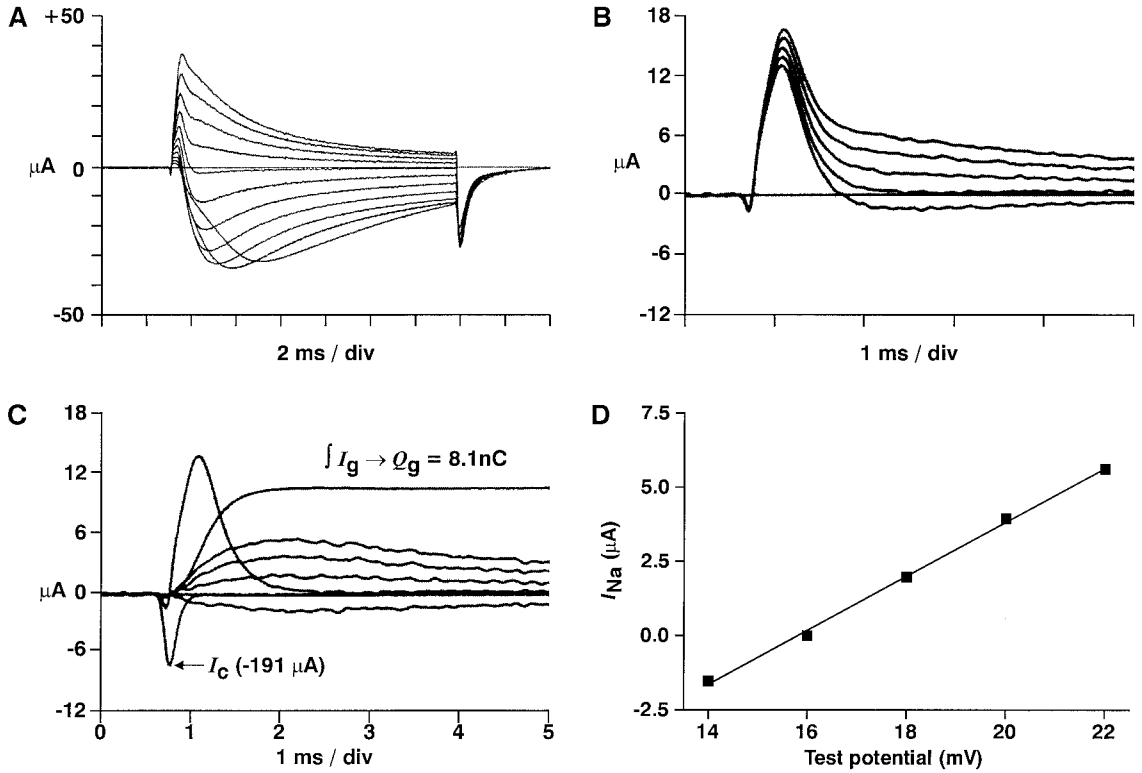

FIGURE 5 Estimation of gating charge and sodium conductance around the sodium reversal potential for high sodium channel expression. (*A*) Simultaneous recording of ionic and gating currents without TTX for test pulses of −40 to +60 mV in steps of 10 mV; V_h − 100 mV. (*B*) Recordings as in *A* but 2 mV steps from +14 to +22 mV, expanded time scale. (*C*) Trace at E_{Na} of 16 mV displays gating current and its integral gives the total gating charge Q_g. Capacitance transient I_c reflects speed of voltage-clamp. The trace at 16 mV subtracted from the other traces leaves the pure sodium currents around E_{Na} (see text). (*D*) Peak sodium currents of *C* plotted against pulse potential; the slope dI_{Na}/dV gives a conductance G_{Na} of 0.91 mS. Cell No. P27S10; temperature 8°C.

For the analysis of ionic conductance, the gating current trace is subtracted from the family of traces around E_{Na} to obtain practically pure ionic currents, since the gating current hardly changes in contrast to the ionic current over this small voltage range (Fig. 5 *C*). The comparison in Fig. 5 *C* of the time courses of the capacitance transient (I_c), $I_{g,t}$, and I_{Na} shows that the clamp is fast enough to record the gating current, which in turn has practically come to zero at the peak time of the sodium current, as expected. The I_{Na} versus voltage plot in Fig. 5 *D* shows that in this experiment the conductance dI_{Na}/dV at E_{Na} was 0.91 mS. It may be noted here that the measured reversal potential is not subject to R_s errors, because no current is flowing but the conductance dI_{Na}/dV of 0.91 mS corresponds to a resistance of 1.1 kΩ, and here an R_s of 200–300 Ω has some effect. This will be discussed below, as well as the question whether E_{rev} represents E_{Na} (*I*/*V* curves Fig. 6 and compiled data of Table 1 in the Discussion).

Quantitative comparison of sodium permeability and gating charge

During the course of the experiments where we recorded the gating current at E_{Na} we repeatedly had to determine E_{Na}. We soon noticed that this reversal potential decreased from initial values ~+40 to +50 mV down to +15 mV, especially when the experiment lasted up to an hour or more. For instance, the two runs displayed in Fig. 5, *A* and *B* were from the same cell and separated by 17 min, while E_{Na} changed from +23 to +16 mV. It could even happen that after one determination of E_{Na} it would decrease by a few millivolts while running an experiment of some 3–5 min. This was manifested by an increasing outward ionic current that contaminated the initially pure gating current. The most likely explanation was a sodium influx either caused by I_{Na} through activated channels or, alternatively, by a small but continuous leak at the holding potential with its large driving force. Below, experimental evidence in support of the latter hypothesis is given. Thus, to obtain the amount of conducting channels we were faced with the problem that the cytoplasmic sodium concentration $[Na^+]_i$, and hence its driving force, would continuously change in one experiment and within the pool of experiments. We, therefore, also used low extracellular sodium concentrations by partial replacement of sodium by the nonpermeating cation choline. In addition, we did not use the sodium conductance for an estimate of the number of open channels, but the sodium perme-

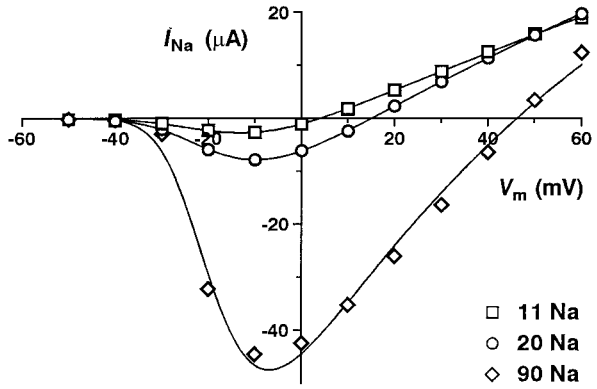

FIGURE 6 Peak sodium currents versus voltage in three different external sodium concentrations fitted by permeability rather than conductance. Recordings for testpulses of −50 to +60 mV in steps of 10 mV, V_h −100 mV, critical R_s compensation, and subtraction of linear components applied as described. External solution was changed by perfusion and contained in sequence 11 mM, 20 mM, and 90 mM $[Na^+]_e$ made from MBS solution and choline$^+$ replacing sodium. The fitted Eq. 5 gave the following parameters for these three $[Na^+]_e$ respectively: E_{Na} equals +4.0, +15.1, and +46.2 mV from which, using the Nernst equation, $[Na^+]_i$ was calculated as 9.4, 11.0, and 15 mM; maximal sodium permeability P_{Na} equals 9.1, 8.6, and 6.6×10^{-9} l/s; V' equals −27.2, −28.1, and −27.2 mV; the slope A equals 11.7, 10.3, and 7.4 mV. Experiment Q19J; temperature 15°C.

ability, which should depend less on the concentration of sodium on either side of the membrane (see Methods).

Fig. 6 shows a validity test for the use of P_{Na} as a figure proportional to the number of activated channels at varying sodium concentrations. The three I_{Na} versus V curves were obtained for pulses between −40 and +60 mV in steps of 10 mV in three different bath solutions to change $[Na^+]_e$ in a rapid sequence from 11 mM to 20, and finally 90, mM. The I/V curves, and especially E_{Na}, changed from +4.0 and +15.1 to +46.2 mV. Assuming the sodium channels to conduct only Na^+ ions, $[Na^+]_i$ was calculated from the Nernst equation as 9.4, 11, and 15 mM, respectively. Should the sub-Nernstian low E_{rev} of +4 mV or +15.1 mV be explained by a partial selectivity for choline, its relative permeability P_{Ch}/P_{Na} would have to be 0.08 or 0.18, respectively, which appears unrealistically high. The internal K^+ also cannot explain the changes of $[Na^+]_i$, but might shift the absolute values slightly by an almost constant amount. The data were fitted by Eq. 5, which combines a Boltzmann equation for voltage dependence of gating with P_{Na} and should be independent of $[Na^+]_{i/e}$. Indeed, maximal P_{Na} is rather constant, being 9.1, 8.6, and 6.6×10^{-9} l/s in sequential order. The midpoint of activation (V' in Eq. 5) being −27.2, −28.1, and −27.2 mV, as well as the indicator of the voltage dependence, the slopes A of 11.7, 10.3, and 7.4 mV do not vary much. They most probably indicate some distortion by R_s errors in the linear and more so in the nonlinear voltage ranges. Taking only dI/dV from the pair of data points across each E_{rev}, one would obtain for G_{Na} 0.39, 0.47, and 0.98 mS, and for P_{Na} 10.0, 8.5, and 8.2 nl/s (note the steeper slope of the data points versus fitted curve). A correction for an uncompensated rest of R_s of 200 Ω (the linear distortion as discussed above) would change G_{Na} to 0.424, 0.518, and 1.22 mS, and P_{Na} to 10.9, 9.3, and 10.2 nl/s. In conclusion, P_{Na} around E_{Na} appears to be a rather good estimate for the number of open channels in varying sodium concentrations, and R_s errors appear to lead to an underestimation of P_{Na} by ~8% for G_{Na} in the range of 0.5 mS and by ~25% in the range of 1 mS.

The next step was to measure I_g and G_{Na} and check whether the ratio of P_{Na}/Q in different cells and conditions was constant. For this purpose, we performed experiments as demonstrated in Fig. 5. E_{Na}, G_{Na} at E_{Na} and $[Na^+]_e$ were used as input for Eq. 4 in order to calculate the maximal permeability P_{Na}. The resulting figures from three batches of injected oocytes are given in Table 1, together with the experimental conditions and cell properties. At 90 mM external sodium, the equilibrium potential E_{Na} dropped substantially to different levels during the experiments and, as calculated from the Nernst equation, $[Na^+]_i$ increased to values of 15 up to 41 mM. In contrast, low external sodium concentration leads to a more stable intracellular sodium concentration at a reduced level (see Table 1).

The ratio of P_{Na}/Q_t, which we initially expected to be constant, clearly varied substantially by more than a factor of 4 within a single batch of oocytes. We noticed that this ratio became smaller when E_{Na} dropped and the calculated $[Na^+]_i$ increased. This is better seen in the graphical representation of the tabulated figures for P_{Na}/Q_t and $[Na^+]_i$ (Fig. 7 *A*; batch 1 in Table 1). The data follow a hyperbolic relation that becomes linear in the log-log plot (Fig. 7 *B*). The increase of $[Na^+]_i$ could also be reversed when after an incubation in 73 mM external sodium concentration this was lowered to 20 mM (experiments P27S10 and P27S11 in Table 1 and asterisks in Fig. 7). The experimentally induced reduction of $[Na^+]_i$ from 39 back to 14 mM occurred within a time of ~20 min and was accompanied by a nearly threefold increase of the P_{Na}/Q_t ratio, pretty close to the overall trend of the data from the whole batch.

From these observations we suspected that oocytes with such a high expression of sodium channels (as derived from I_g) would leak some sodium ions into the cell along the concentration gradient. This might occur either continuously, through a few open channels but a large driving force at the holding potential of −100 mV or, in addition, due to the inflow during the pulses. This would force the cell to actively pump sodium ions out for its homeostasis, which represents an energetic stress for the cell. As a result, the permeability of some channels would be down-modulated by an as yet unknown mechanism, whereas the gating charge of these channels remained undisturbed. Therefore, we hypothesized that a similar sodium load also stresses the cells during the days of incubation, because at the typical resting potential of −15 to −30 mV it is rather likely that a

TABLE 1 Sodium channel conductance, permeability, and gating charge at sodium reversal potential; estimated number of channels per whole *Xenopus* oocyte

Expt. (dpi)	C_m (nF)	T (°C)	$[Na^+]_e$ (mM)	E_{Na} (mV)	$[Na^+]_i$ (mM)	dI/dV (mS)	P_{Na} (nl/s)	Q_t (nC)	P_{Na}/Q_t ($l \cdot s^{-1} \cdot C^{-1}$)	$N_{i,o}$ ($\times 10^6$)	N_g ($\times 10^6$)	$N_{i,o}/N_g$ (%)	Q_n/Q_t (%)
Batch 1													
P21S03 (4)	248	9	90	25	33	0.32	1.59	3.40	0.47	27	2656	1.0	21*
P21S04 (4)	248	9	90	20	41	0.39	1.73	3.30	0.52	30	2656	1.1	33*
P22S06 (5)	256	10	90	40	18	1.10	7.82	4.20	1.86	135	3281	4.1	39
P23S03 (6)	216	8	90	36	21	0.56	3.61	1.60	2.25	63	1250	5.0	50
P25S02 (8)	260	8	90	43	16	1.16	8.90	7.30	1.22	153	5703	2.7	47
P25S06 (8)	260	8	90	34	22	1.12	6.87	5.20	1.32	118	4063	2.9	44
P27S03 (10)	270	8	20	8	15	0.54	8.26	3.70	2.23	143	2891	4.9	41
P27S04 (10)	270	8	20	6	16	0.49	7.19	3.40	2.12	124	2656	4.7	38
P27S10 (10)	270	8	73	16	39	0.91	4.53	7.00	0.65	78	5469	1.4	54
P27S11 (10)	287	8	20	9	14	0.59	9.22	5.30	1.74	159	4141	3.8	26*
P27S12 (10)	287	8	20	8	15	0.64	9.79	4.90	2.00	169	3828	4.4	24*
Batch 2													
P22O04 (8)	244	15	90	15	50	0.57	2.29	1.58	1.45	39	1234	3.2	38*
P29O10 (15)	274	15	90	20	41	1.50	6.71	5.10	1.32	116	3984	2.9	49*
P29O13 (15)	249	15	90	15	50	2.00	8.03	4.55	1.77	139	3555	3.9	ND
P01N04 (18)	183	15	90	40	19	0.62	4.41	1.58	2.79	76	1234	6.2	65*
Batch 3													
P08D04 (6)	284	15	10	4	9	0.19	5.47	2.10	2.61	94	1641	5.7	52*
P08D16 (6)	226	15	10	9	7	0.63	20.08	1.77	11.34	346	1383	25.0	ND
P09D01 (7)	252	15	10	0	10	0.18	4.80	2.16	2.22	83	1688	4.9	42*
P09D14 (7)	285	15	10	10	7	0.52	16.92	5.07	3.34	292	3961	7.4	53*
P09D16 (7)	285	15	10	10	7	0.92	29.93	5.69	5.26	516	4445	11.6	77*
Mean†	258					0.57	8.41	3.95	2.42	145	3086	5.3	44
SD	27							1.78			1388		14
(SD)						0.45	6.83		2.36	118		5.2	

(dpi) Days after cRNA injection.
*Recovery time 1 ms, else 2 ms.
†Mean of all figures of a column (also for all Q_n/Q_t; 1 and 2 ms recovery). Standard deviations SD and (SD): the latter contains data from ionic currents and varies more than SD. Dimension of permeability P in l(iter)/s(econd). $N_{i,o} = P_{Na}/(5.8*10^{-17}$ l/s); (single channel permeability).

fraction of channels stays open and the electrochemical driving force for sodium leads to a persistent sodium influx. Consequently, to reduce the cytoplasmic sodium load, we added 2 μM TTX to the incubation solution. For the voltage-clamp experiment, the cells were washed and transferred into MBS without TTX and with 90 or 10 mM sodium. This resulted in an increase of the permeability/gating-charge ratio which, however, still was dependent on the internal sodium concentration (Table 1, Fig. 7 *B*; batches 2 and 3). For the pool of our data, the P_{Na}/Q_t varied by a factor of 10–20, which is much larger than simple experimental variation and, therefore, indicated a clear dependence on the influx of sodium or its cytoplasmic accumulation.

Experiments to compare sodium influx and increase of cytoplasmic sodium

The above-calculated free cytoplasmic sodium concentration from E_{rev} indicates a substantial increase of $[Na^+]_i$ during the experiment. As suggested, this might be due to leak at holding potential or I_{Na} during the pulses. We have

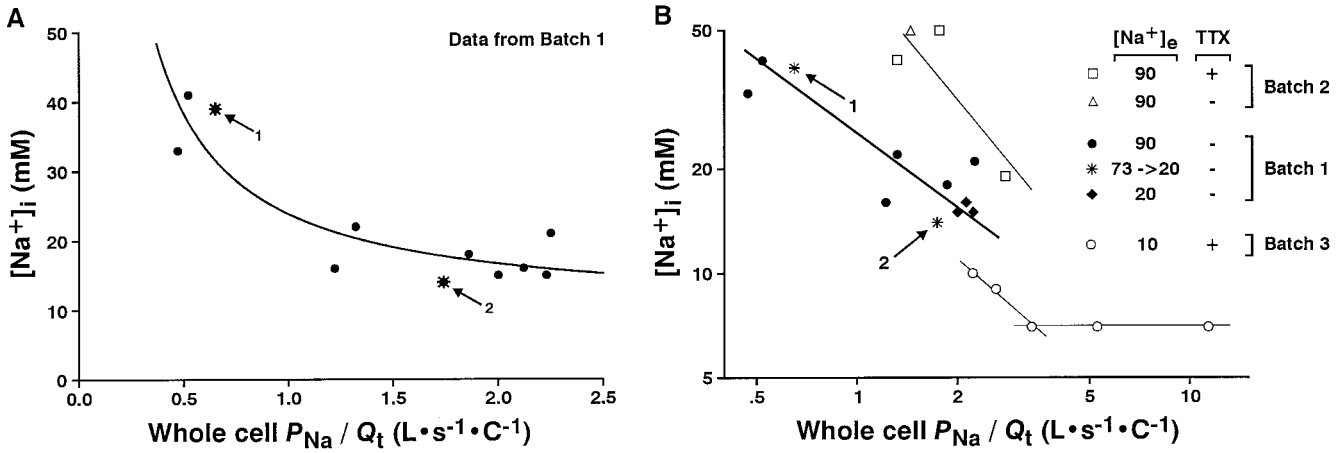

FIGURE 7 Graphical presentation of the varying ratio of sodium permeability and gating charge versus the corresponding internal sodium concentration, from data in Table 1. (*A*) Batch 1, no TTX during time of sodium channel expression. Asterisks mark two experiments at the same cell with 73 mM (*arrow 1*) and 20 mM (*arrow 2*) $[Na^+]_e$ in the bath. The fitted hyperbola is of the form $Y = A/X + B$. (*B*) Log-log plot of the same data of batch 1 in the linear plot (*filled symbols*) and additionally the data from batches 2 and 3 in Table 1 (*open symbols*). Inset indicates $[Na^+]_e$ in the bath and whether 2 μM TTX was added during expression. Lines were fitted by eye.

performed the following checks on this: 1) comparison of the integrated leak during the experiment with the calculated change of $[Na^+]_i$; 2) use the inactivation deficient mutant IFM/QQQ and application of repeated long pulses to produce a substantial influx by pulses; 3) comparison of agarose-cushion electrodes and open-tip ones filled with NaCl for their leak into the center region of the oocyte and check the resulting changes in E_{rev}. For all these calculations it was important to know the freely accessible space in an oocyte. According to the in-depth studies on amphibian oocytes by Horowitz (e.g., Horowitz and Paine, 1979) Na^+ distributes quickly into the sucrose-accessible space. This cytoplasmic space represents ~30% of the cell water, while the vesicular structures, most prominently the yolk vesicles, may actively accumulate sodium (Dick and Fry, 1975). For the oocytes used in our experiments of 1.3 mm diameter and a calculated volume of 1.15 μl we assume an average water content of 75% and obtain 0.25 μl for the freely accessible space. Fig. 8 *A* shows for a typical experiment the leak-current *I*-hold at V_h of −100 mV during the whole experiment. Assuming this current to be all Na^+-influx into the freely accessible space, the resulting change of $[Na^+]_i$ is calculated. The filled circles in Fig. 8 *A* were measured over the time where also E_{Na} (E_{rev}) was determined and used to estimate $[Na^+]_i$ by the Nernst equation (Fig. 8, *B* and *C*). Between the two open circles marked by 1 and 2 asterisks, TTX was applied to the bath. In this experiment most of the leak was blocked, suggesting that indeed the leak would be carried by Na^+ ions through sodium channels. (At present, we cannot be conclusive about the TTX-sensitive part of the leak because we normally extended the experiments until the leak was too high for reasonable clamping.) Then, the mean leak integrated over this period was 0.32 μA and the resulting change in $[Na^+]_i$, or as indicated in Fig. 8 *D*, Δ[ion]/min in the accessible space would be 0.77 mM/l/min. This was then directly compared with the change of $[Na^+]_i$ as obtained from the data in Fig. 8 *C*, i.e., 0.26 mM/l/min. The results of similar experiments with a smaller and a larger leak are shown in Fig. 8 *D*. In experiment 3 (Fig. 8, *D* and *E*) G_{Na} was also determined several times during the marked increase of internal sodium and P_{Na} calculated. G_{Na} showed a slight decrease and the plotted P_{Na} showed a clear inverse relationship similar to the pool of experiments in Table 1. This will be further treated in the Discussion.

The change of internal free sodium due to influx was always found to be ~2–4 times larger than that obtained from the change in E_{rev}. The following explanations were mainly considered. 1) The seemingly too large leak influx may not consist only of Na^+ or 2) distribute into a larger freely accessible space than assumed, or 3) some of the increased sodium is pumped actively back into the bath or into the intracellular vesicles. The active pumping appears to be the most likely mechanism. The percentage of freely accessible space is rather well documented and shows only little variation. As a further check to let Na^+ specifically enter the cell, we used the noninactivating mutant IFM/QQQ at high expression. While the normal I_{Na} of wild-type at a relatively low stimulus rate during an experiment had a negligible influx, with this mutant 200-ms-long pulses at a frequency of 1/s for 1000 sweeps were applied. In this way we obtained a substantial influx from well-defined current plateaus of exactly measurable size (4–10 μA) for 200 ms followed by a duty cycle of 800 ms, which allowed for diffusion. In several experiments we found the change of $[Na^+]_i$ due to influx to be again 2–4 times larger, i.e., 1.5–3 mM/l/min versus 0.4–0.8 mM/l/min as obtained from the change in E_{rev}. It thus appears very likely that the Na^+ influx provokes a pump activity of ~1–2 mM/l/min with a

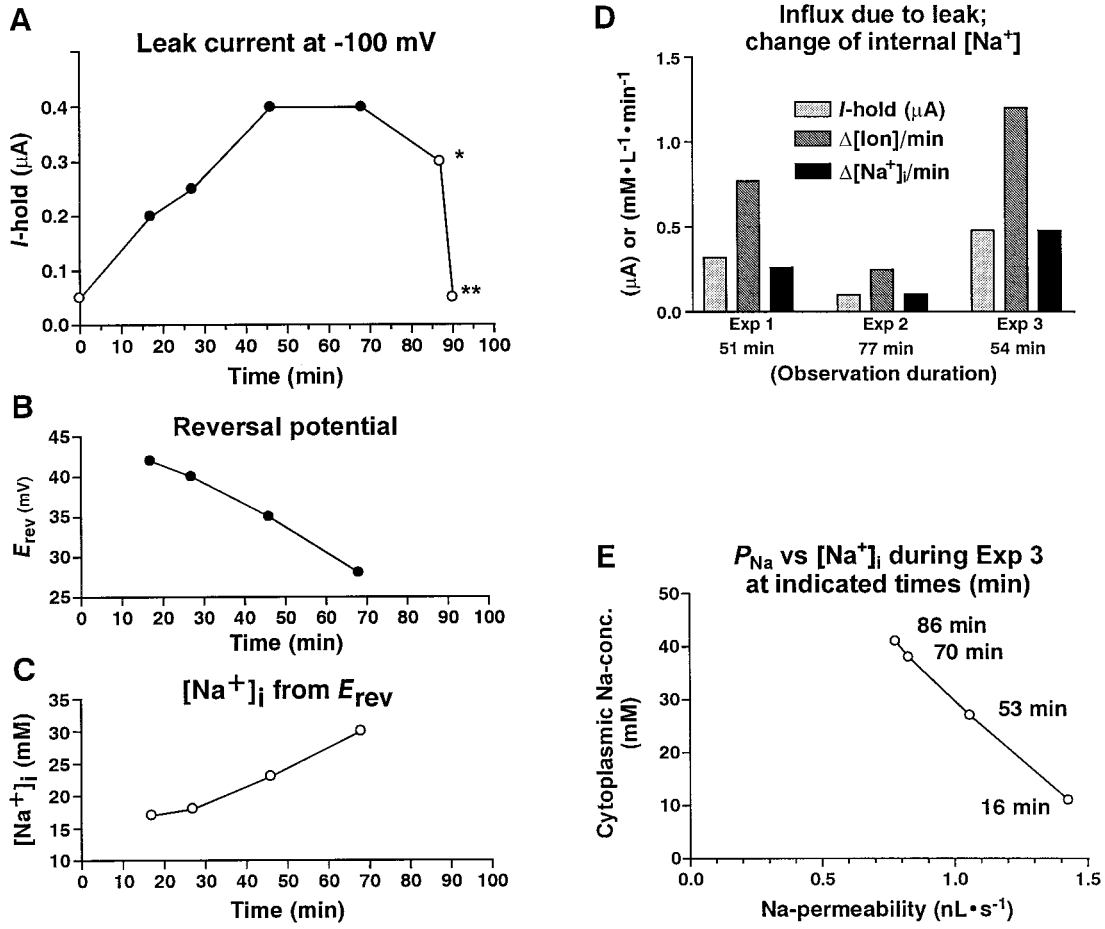

FIGURE 8 Comparison of leak current at holding potential and free internal sodium $[Na^+]_i$ as calculated from the observed reversal potential E_{rev} for three experiments done in constant $[Na^+]_e$ of 90 mM. (*A*) Experiment 1 with typical leak or holding current of medium size (*I*-hold) at V_h of −100 mV, typically increasing during the experiment. It could be almost totally blocked by TTX at the end in this experiment (TTX given between the circles marked by ∗ and ∗∗). The filled circles correspond to the time when E_{rev} was also measured as given in (*B*) for the calculation of $[Na^+]_i$ using the Nernst equation (*C*). (*D*) From the mean *I*-hold, 0.32 μA for experiment 1, distributing into a free accessible space of 0.25 μl in the oocyte (see text), the expected change of ion-concentration per minute is indicated and compared to the observed change in free $[Na^+]_i$ as obtained from the data in *C*. Similarly obtained data are shown for 2 other experiments with either a small and constant leak of ~0.1 μA (experiment 2) or a rather large leak (experiment 3). (*E*) For experiment 3 the changing figures for P_{Na} around E_{rev} were determined and displayed versus the cytoplasmic free $[Na^+]_i$ as calculated at the indicated times from the interpolated E_{rev}.

stoichiometric consumption of 1:3 of 1–2 mM ATP/min in order to keep the internal sodium at low levels. In further experiments using 3 M NaCl-filled coarse tip electrodes with or without an agarose cushion we could demonstrate that without agarose a fast leakage of sodium in the central region leads to changes of E_{rev} that indicated a change of $[Na^+]_i$ under the membrane by 3–4 mM/l/min. While these experiments demonstrate the fast diffusion within the cell, they did not allow us to control and quantify the influx and concentration as well as in the voltage-controlled QQQ mutants. In these latter experiments we could further observe during the quantified Na^+-influx and decrease of E_{rev} that the conductance d*I*/d*V* at E_{rev} became smaller, which will be treated further in the Discussion when estimating the number of open channels from either G_{Na} or P_{Na}.

Properties of the unexpectedly large gating current

Our results indicated the presence of a large proportion of channels with a very low open probability that produced gating current. Therefore, we had to consider and to exclude whether 1) the gating current would be changed to an abnormal gating current, or 2) that most of the channels would remain in normal inactivated states, not producing ionic current but still gating current by the nonimmobilized parts of the voltage sensors. To check on this, we performed double-pulse experiments in order to compare the recovery of ionic- and gating-currents and the size of immobilization. As known from other preparations and shown schematically in Fig. 2, the gating current of the inactivated and immobi-

lized channels represents 40–50% of the total gating current produced by recovered channels, has faster kinetics, and no slow rising phase. We checked for this by applying optimal recording conditions, small asymmetry, and a low temperature of 8°C to slow the fast gating-current in relation to the speed of the clamp (given by the capacitance transient). The recording was done in quick succession for the gating current at E_{Na} and the ionic current at a potential ~10–30 mV below E_{Na} to get sodium currents of a size not subject to R_s errors. It has to be recalled that the recovery time course is determined by the potential during the interpulse interval (−100 mV) and not by the potential of the test pulse. Fig. 9, *A* and *B* show the superimposed traces of I_{Na} and I_g of the test pulse for a series of recovery periods of 60, 1, 2, 3, 5, . . . up to 60 ms after the same inactivating prepulse. For the shortest intervals there is still the gating-current from those channels switching between inactivation states. Frequently, there is some ionic-current when not all channels are inactivated that shows up as a noninactivating plateau of ionic current. With increasing recovery more and more channels produce ionic-current, which activates and inactivates in the normal way. The corresponding I_g traces seem to grow faster initially because during the shortest gap even the fast equilibration between the inactivated states could not finish and, consequently, $I_{g,on}$ is small. The full gating-current of immobilized channels can be seen after 2 ms recovery (3rd trace) and clearly shows a steeper and shorter time course than that of fully recovered channels with a prominent rising phase. This corresponds very well to the results of similar experiments where high-resolution gating-currents were recorded in the squid giant axon (Greeff et al., 1982).

For further analysis of the recovery experiments we compared the time course of recovery of $I_{Na,peak}$ and the integrated gating charges Q_g. In Fig. 9 *C* these data are shown individually versus the recovery time, while Fig. 9 *D* displays the same data as a phase plot of Q_g versus $I_{Na,peak}$. As can be seen in the phase plot, after the shortest recovery gaps of 1 and 2 ms, both quantities recover in parallel, as indicated by the straight line. This corresponds to similar time constants of 11.4 and 12.8 ms for Q_g and $I_{Na,peak}$, respectively. In this particular experiment the percentage of nonimmobilized gating current (Q_n) from inactivated channels being 4.6 nC after 3 ms or 4.0 nC extrapolated back to

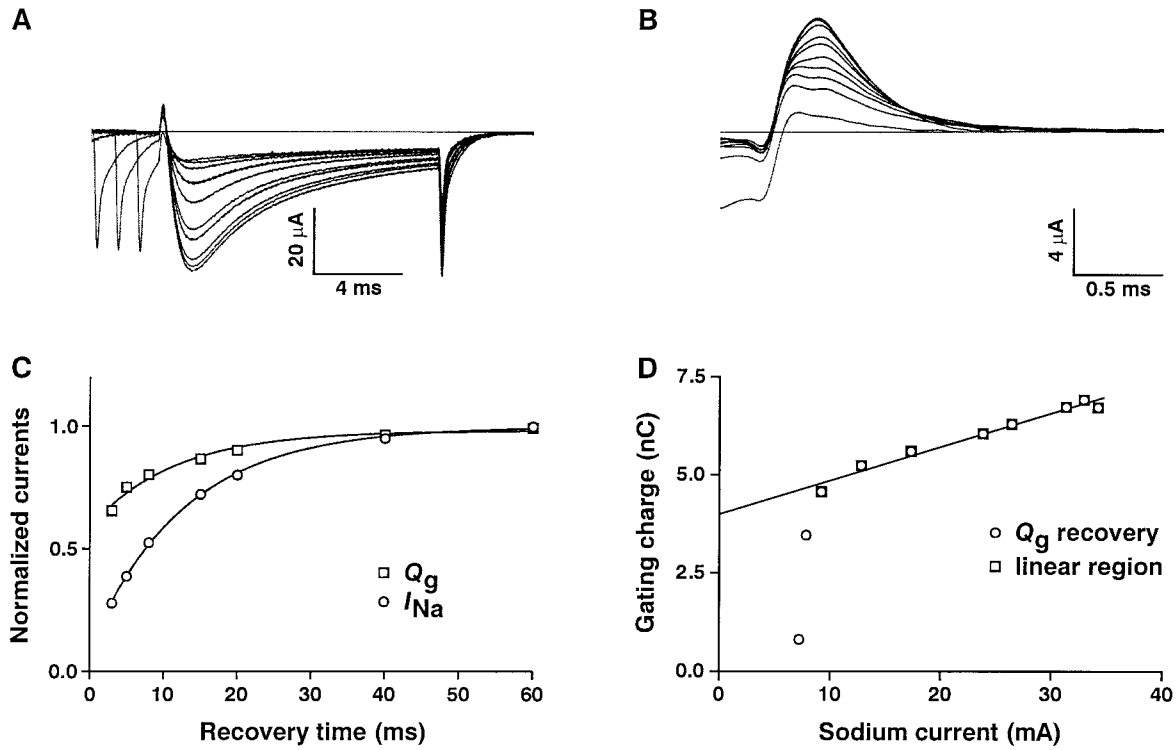

FIGURE 9 Comparison of recovery of sodium ionic- and gating-current from inactivation or immobilization, respectively. (*A*, *B*) Single cell experiment; no TTX had been used and the recordings were done within a few minutes: gating currents at E_{Na} of +42 mV first (*B*); and 12 min later at a test potential of +10 mV the ionic currents (*A*). Otherwise identical protocols: inactivating prepulse to +40 mV for 20 ms; V_h and recovery at −100 mV, recovery gaps were (in ms) 60, 1, 2, 3, 5, 8, 15, 20, 40, and 60; linear subtraction pulses between −100 and −130 mV. Critical R_s compensation; duration of the capacitance transient (not shown) gives the speed of the clamp and is reflected in the fast rise of I_g, which is followed by a genuine slow rise. (*C*) Recovery of peak sodium current (I_{Na}) and integrated gating currents (Q_g), normalized to maximal values; single-exponential fits to the plotted data (except 1 and 2 ms points, compare *D* and text) gave τ_{rec} of 12.8 and 11.4 ms for I_{Na} and Q_g, respectively. (*D*) Isochronic plot of Q_g versus I_{Na} for all data points (*circles*), 3 to 60 ms recovery data points are close to linear fit (*squares*). Experiment P25S2; MBS-solution; temperature 8°C.

zero recovery time is 57 or 66%, respectively, in comparison to the fully recovered gating-current. In order to check on this more thoroughly we calculated this ratio for the experiments from Table 1. The average ratio of Q_n/Q_t is 44 ± 14% (SD, n = 18) which agrees well with the above-quoted figures from other preparations (Armstrong and Bezanilla, 1977; Greeff et al., 1982). Note that in batch 1 at 8°C, 1 ms recovery gave a percentage of 21 to 33% (*Q_n/Q_t marked in Table 1) which supports the finding of Fig. 9 *D*, namely that at this temperature even Q_n does not fully recover; in batches 2 and 3 at 15°C a 1-ms recovery is sufficiently long. The important conclusion is that we certainly do not see a variation in Q_n/Q_t corresponding to the 5- to 20-fold variation in the P_{Na}/Q_t ratio. This suggests that the unusually large gating currents behave normally with respect to immobilization and recovery, as will be treated further in the Discussion.

Furthermore, we tested the time course of I_g at different voltages for its characteristics and the integrated charge for saturation at higher voltages to exclude any nonsubtracted linear contamination. Fig. 10 *A* displays a family of gating currents for pulses of −60 to +80 mV in steps of 10 mV at high time resolution. The traces show the typical properties known from squid axon gating currents: a fast rise limited by the charging time of the membrane capacitance, which is followed by a genuine, typical slower rise time that becomes faster at higher voltages (compare with Fig. 9 in Greeff et al., 1982). At 15°C a concentration of 2 μM TTX did not fully block the ionic current, causing some ionic contamination visible in the baseline deviations. This contamination distorts somewhat the integration of I_g for obtaining Q_g, especially between −30 to 0 mV where the ionic currents also are largest. Without this contamination the Q/V curves saturate above 0 mV, as the examples for cells matured in TTX-free and TTX-containing incubating solutions show (Fig. 10 *B*).

DISCUSSION

This paper has a methodological aspect because it shows the constraints and delivers protocols for the recording and identification of sodium channel-gating currents with a fast two-electrode voltage-clamp from whole *Xenopus* oocytes. However, we describe a hitherto unknown down-regulation of the sodium channel permeability that was detected by correlation of gating- and ionic-currents at single oocytes. The TEVC technique is a relatively easy and fast method for screening and functional studies of mutant channels. We now have shown that it also allows the recording of well-resolved gating currents at an adequate resolution. This technique had already been profitably used to study sodium channels with respect to inactivation and charge immobilization using mutations in S4D4 (Kühn and Greeff, 1999). In comparison to the cut-open oocyte method (Stefani et al., 1994; Stefani and Bezanilla, 1998) the two-electrode preparation, although easier to handle, does not allow changing the cytoplasmic solution. Concerning the clamp speed, the cut-open method may at present be the slightly faster clamp because we had to compromise somewhat to achieve a more linear clamp, and so avoid asymmetries that would distort the gating current. As Fig. 3 shows, however, a comparable speed can also be achieved, but we will then have to improve further on the linearity of the clamp system. Another successful method for recording sodium I_g is the macropatch method, especially for gating-current noise

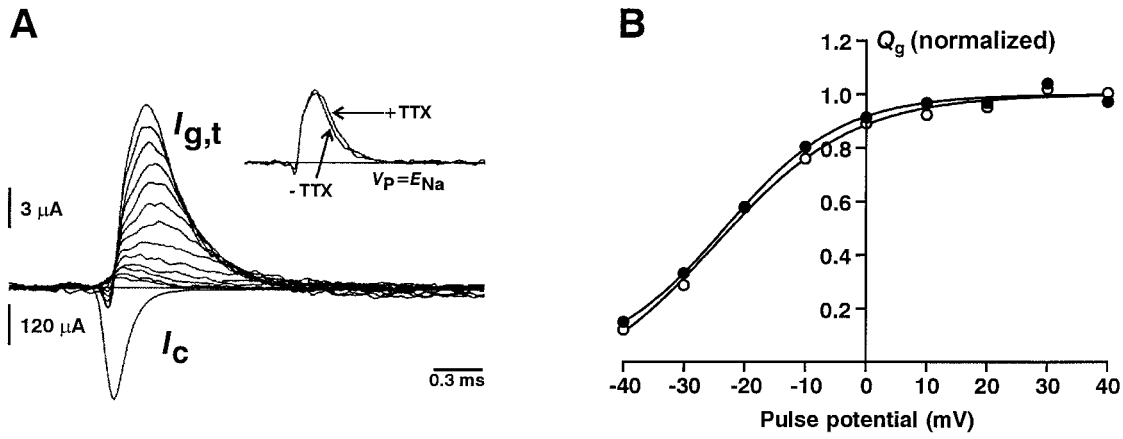

FIGURE 10 Voltage-dependence of the time course of sodium channel-gating current at high temporal resolution and Q/V-curve showing saturation at high depolarization. (*A*) Gating currents for test pulses of −60 up to +60 mV in steps of 10 mV. Fast rise followed by slow rising phase. *Inset:* superimposed I_g traces obtained at +40 mV ($\cong E_{Na}$) in TTX and without TTX (no net I_{Na} at E_{Na}). (*B*) Gating charge from integrated I_g traces for pulses over the range of −40 to +60 mV from two oocytes; one had been incubated in MBS solution without TTX (*filled circles*) during expression and TTX only for the experiment, the other one with 2 μM TTX added throughout (*open circles*); linear subtraction pulses between −120 and −150 mV. Experiments P01N3 and S6A10,12; temperature 15°C.

analysis where the number of channels should not be too large (Conti and Stühmer, 1989).

Already in our first estimations the gating charge appeared to be up to 20 times larger than expected from the sodium ionic currents, which prompted us to examine in detail both the conducting and gating properties of the sodium channels and to search for possible conditions responsible for the observed mismatch. Before trying to estimate absolute channel numbers, the amount of gating charge per oocyte is initially considered and compared with that from potassium channels expressed in oocytes of the same batch. *Shaker* potassium channel cDNA cloned into the same high-expression vector as the sodium channel (a gift from Dr. Ligia Toro) was mutated to obtain the nonconducting channels as elsewhere used to study potassium channel gating currents (mutation W434F; Perozo et al., 1993). In Fig. 11, a comparison of whole-cell recordings obtained with our optimized TEVC is shown from oocytes injected with cRNA either coding for wild-type rBIIA sodium channels or W434F potassium channels. Recordings for a family of step depolarizations were taken at different temperatures (7.5, 15, and 22.5°C). The gating-currents from both channel types are faster at higher temperature, as expected, and both depend in a similar manner on voltage. In contrast, the capacitance transients and the small asymmetries are practically unchanged at different temperatures. These results confirmed further that we in fact were recording sodium channel-gating currents and that the oocytes possess the capacity of producing that many channels.

Next we attempt to estimate the number of channels first from the gating current because this requires fewer assumptions, i.e., only a figure for Σq, the total gating charge displaced in a single activated channel assumed to be 8 e_o (see above, Eq. 2). The numbers of gating channels N_g obtained in this way are given in Table 1 and range between 1.3 and 5.7×10^9 channels per oocyte, with an average of $3.1 \pm 1.4 \times 10^9$ channels. This number corresponds to an amount of ~1 ng channel protein per oocyte, which is well within the capability of stage VI *Xenopus* oocytes for synthesizing membrane proteins (Richter and Smith, 1981; Galili et al., 1988). A further interesting quantity is the channel density per membrane area. The oocyte membrane is ~5 times larger than the surface of a simple sphere of 1.3 mm diameter due to the extensive microvillous structure. A good estimate may be taken from the membrane capacitance of ~250 nF/oocyte in our case, which indicates an area of 0.25 cm^2 of a standard lipid bilayer with 1 $\mu F/cm^2$. This gives for 4×10^9 channels a density of 160 channels per μm^2 effective membrane, a figure which is rather close to 180 (Bekkers et al., 1986) or 330 sodium channels per μm^2 (Conti et al., 1975) found in native excitable membrane of squid giant axons.

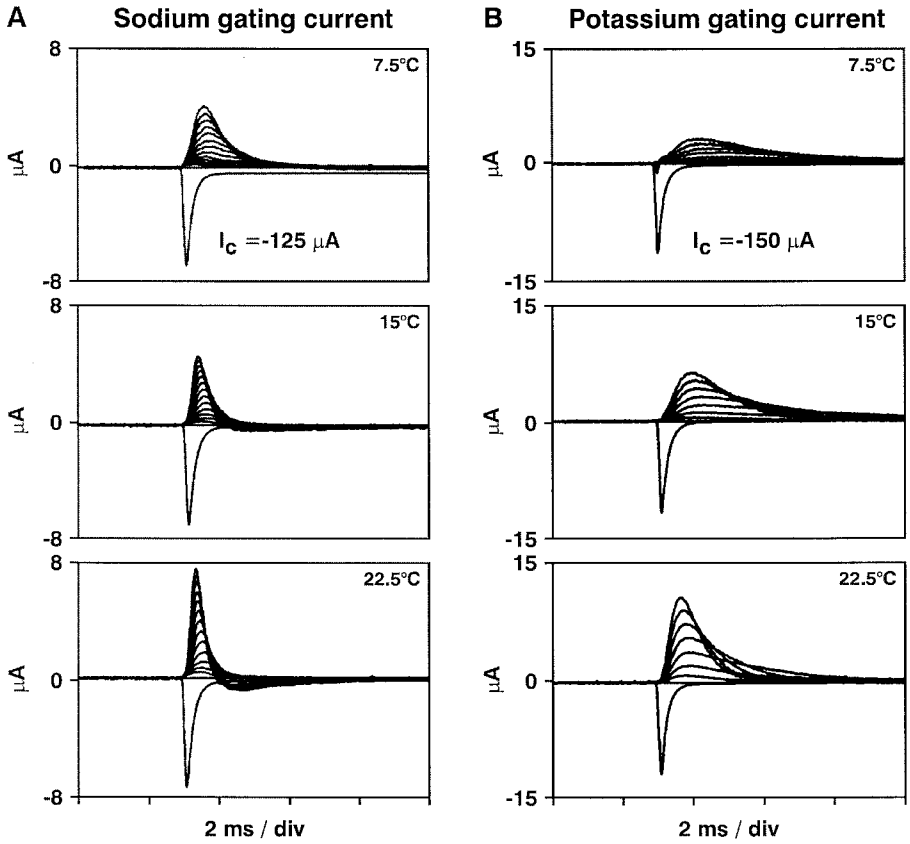

FIGURE 11 Comparison of sodium (rBIIA) wild-type channel and potassium channel (*Shaker* W434F) gating currents recorded with fast TEVC at different temperatures, as indicated. (*A*) Sodium-gating currents for test pulses of −60 to +60 mV in steps of 10 mV; capacitance transients indicate identical clamp speed at the different temperatures. Note that in MBS the blocking effect of 2 μM TTX is much better at 7.5 than at 22.5°C. (*B*) Potassium gating currents in MBS at similar clamp speed and temperatures as used in *A*; testpulses −60 to +60 mV in steps of 20 mV. The kinetics of the potassium channels are ~5 times slower than those of the sodium channels. Experiments PFKNaG, P13N6–9.

When attempting to estimate the channel number from the ionic currents, there are several factors and assumptions to be considered. A first crude estimate may be obtained by simply dividing a peak sodium current of ~50 μA by a single channel current of 0.9 pA (Goldin, 1991), both obtained in ~90 mM external sodium and in a similar voltage region of −30 to −10 mV; this would give 56×10^6 open channels at peak time. However, a macroscopic ionic current of that size may be distorted by R_s errors, as discussed in the Results. This was minimized in our case by obtaining the conductance dI/dV around the reversal potential. Dividing the mean figure of 0.56 mS (Table 1) by a typical single channel conductance of 11 pS for *Xenopus* oocytes (Auld et al., 1988) one arrives at a similar figure of 48×10^6 open channels at peak time which, however, will be revised (see below). It assumes a normal concentration of cytoplasmic Mg^{2+} (whole-cell conditions for our experiments as well as for the quoted single channel figure from Auld et al., 1988 or from Goldin, 1991) while at zero Mg^{2+} the conductance is ~15 pS (Pusch et al., 1989). In our study we had to deal with different sodium concentrations and nonsymmetrical distributions on the internal and external side of the membrane and, therefore, we preferred to use the permeability as obtained by Eq. 4. By dividing the maximal permeability P_{Na} obtained at E_{Na} by the single channel permeability we obtained for the number of channels that are open at peak time ($N_{i,o}$) a mean of $145 \pm 118 \times 10^6$ (Table 1). This figure is about three times larger than the current- or conductance-based estimates above. Here, one has to recall that conductance depends on the ionic concentration and that permeability is meant to account for it. It is interesting to separate the figures of Table 1 for each external sodium concentration of 90, 20, and 10 mM. For each the mean G_{Na} obtained is (in mS) 0.94, 0.57, and 0.49, respectively; likewise, P_{Na} is (in nl/s) 5.2, 8.6, and 15.4 while Q_t is rather constant with figures of (in nC) 3.8, 4.3, and 3.6. Looking now again at the number of open channels obtained from G_{Na} or P_{Na} for $[Na^+]_e$ of 90 mM one obtains from permeability 90×10^6 channels (mean $N_{i,o}$ in Table 1 for 90 $[Na^+]_e$) and from the mean conductance of 0.94 mS divided by 11 pS a figure of 86×10^6 channels. Thus, both methods now come to similar results. This should be so by definition, if the correct single channel slope conductance at the actual E_{rev} and ionic concentrations is taken. For the 90 mM case and a mean E_{rev} of 29 mV the slope conductance at E_{rev} obtained by Eq. 4 (Fig. 1) would be 10.8 pS for the known single channel properties, i.e., close to the 11 pS assumed in the first estimate above. Thus, at the higher $[Na^+]_i$ and lower E_{rev} the slope conductance increases in comparison to Fig. 1 and equals the generally assumed value for the cord conductance. The conclusion is that the factor three obtained above for the total means comes from the divergence of G_{Na} and P_{Na} at lower sodium concentrations on both sides of the membrane, but always assuming 11 pS for the single channel conductance.

Despite many critical comments on the applicability of P_{Na} as an estimate proportional to the number of open channels independent of voltage and ion concentrations, it appears to us still the most reliable method. Under Fig. 6 we have discussed the experimental evidence for changes in external sodium. With respect to the internal sodium concentration and its effect on conductance, we could rather convincingly show that the estimation of changes in $[Na^+]_i$ can be well estimated from E_{rev}, although the absolute figures might have a shift due to a partial selectivity of Na^+ channels for K^+. This is also supported by the results of an often-quoted study on the node of Ranvier that critically examines the applicability of the independence principle and the GHK equation (Fig. 5 in Hille, 1975). The change of external sodium to 232, 116, and 58 mM resulted in E_{rev} values of 55.4, 39, and 22.6 mV, and we would calculate for $[Na^+]_i$ figures of 23.7, 24.8, and 25.6 mM, which as would be expected for this preparation, are rather constant. The absolute figures may not be correct due to a nonperfect selectivity of the channels for sodium, but the change in free Na^+ in which we are interested would thus be well detected. The quoted study arrives at a relative permeability for P_K/P_{Na} of 0.08 such that, e.g., 100 mM $[K^+]_i$ would appear as 8 mM Na^+. In another study on rat skeletal muscle sodium channels expressed in *Xenopus* oocytes a lower figure for P_K/P_{Na} of ~0.02 was found (Chiamvimonvat et al., 1996). In our experiments $[K^+]_e$ is constant; therefore, in order to account for the observed changes in E_{rev}, $[K^+]_i$ would have to change by an amount of 12–50 times more than our calculated changes for sodium, which seems very unrealistic. The quoted study of Chiamvimonvat et al. (1996) and a study by Pusch (1990) on rat brain II sodium channels show the applicability of the GHK-equation for asymmetrical sodium concentrations. Especially in the latter paper it is clearly shown that dI/dV checked by tail-currents is reduced across E_{rev} for 30//125 mM Na^+, but does not change if $[Na^+]_i$ is also 125 mM and is fitted well by the GHK-equation in 0 Mg^{2+}. In conclusion, there is much evidence that the single channel conductance (dI/dV) should increase if either the external or the internal sodium concentration is higher, which is accounted for by using P_{Na}. Therefore, if we find at increasing levels of internal Na^+ a constant or even decreasing dI/dV (see also Results under Fig. 8 *E*) the most likely interpretation is a decrease in the number of conducting channels.

Whatever method is used to estimate $N_{i,o}$, it is definitely much lower than the number N_g obtained from the gating charge. This may be expressed as an overall open probability $N_{i,o}/N_g$ of 1–5% at elevated internal sodium and 5–25% at low internal sodium (Table 1). Here, we propose to take into account that normal sodium channels have an open probability p^o of ~0.5 at peak time and at higher potentials (see Eq. 6 and its discussion and quoted references). Accordingly, we separate the overall open probability into the product of p^o equal to 0.5 (channels with normal open

probability) multiplied with F^a, the variable factor between 0 and 1 indicating the fraction of normal channels. Then F^a varies from 0.02 to 0.1 or 0.1 to 0.5 for different internal sodium concentrations, respectively, and would give the fraction of all channels that contribute to the ionic current with normal p^o of 0.5. This interpretation appears reasonable because the ratio of conducting channels to gating channels obviously varies with changed cytoplasmic sodium concentrations as if being modulated in some way. Thus, we suggest that the very small ionic conductance in relation to the gating current is not due to a reduced single channel current amplitude but rather to a variably reduced open probability, which again may be split into a small fraction F^a of normally conducting and gating channels, and a fraction $(1 - F^a)$ with a very low or even zero probability of opening the pore, but still normal gating current. In other words, there may be a fraction of channels that are silent with respect to ionic conductance but not with respect to gating current. We further conclude that the calculation from the gating current counts more or perhaps all of the channels in the membrane, while the calculation from the ionic current certainly underestimates the number of expressed channels, especially under raised internal sodium. To us it appears plausible that the pores of the modulated sodium channels are blocked while the gating machinery remains intact, because the voltage sensors are distributed in the channel protein and will hardly be stopped altogether. There is an early study on calcium channels that we know to be structurally closely related to sodium channels, which also demonstrates a varying ratio of gating- to ionic-current under modulation by a β-subunit (Neely et al., 1993). Recent studies in transfected cells show for calcium channels that the β1A-subunit increases the ratio of G_{max} to Q_{max} by favoring channel opening (Kamp et al., 1996; Jones et al., 1998). Another study on the same preparation demonstrates the usefulness of correlating gating- and ionic-currents for the study of calcium channel inactivation (Jones et al., 1999). The main issue of our study is not so much the absolute ratio of N_i/N_g, but the nearly 20-fold change of this ratio. The absolute ratio would change by a constant factor for all data if for Σq not 8 but 12 e_o would be assumed (as reported consistently for K^+ channels and also proposed for Na^+ channels, see above). Then, F^a would grow from the maximal figure of 0.5 to 0.75. Taking further into account the linear R_s error around E_{rev} as discussed in Fig. 6, G_{Na} and P_{Na} would have to be increased. For the largest figure in Table 1 in batch 3 the correction would change the ratio by 10–25% depending on G_{Na}, and for that experiment F^a might reach unity; but the majority of the tabulated values still remains far below. The hyperbolic dependence on $[Na^+]_i$ in Fig. 7 would remain because the large figures in Table 1 for P_{Na}/Q_t would be increased more than the small ones. The correction has not been applied because the exact R_s figures are not known for each experiment.

As shown, our findings depend on the relevant figure for the total gating charge per single channel (Σq in our notation or Δq in Sigg and Bezanilla, 1997) but vice-versa also have some impact on estimations of it. This quantity is of relevance for the modeling of channel function (Almers, 1978; Sigworth, 1995; Hirschberg et al., 1995; Sigg and Bezanilla, 1997; comment by Horn, 1996). We do not intend an in-depth discussion on Σq here, but would like to point out that if we would divide the total gating charge Q_t by the number of conducting channels $N_{i,o}$, we would arrive at far too large figures for Σq since—as shown in this study—the gating current from the "silent" channels would erroneously be included. This may in some way be compared to the term "peripheral" charge suggested by Sigg and Bezanilla (1997) who show in their theoretical study the constraints for estimating Σq by methods like the "limiting slope" or "*Q*/*N*" procedures. In our study we were forced to use high expression of channels and are not able to decide whether our conclusions also apply for channels at the lower expression levels used in other studies. However, our findings may be taken into account in studies where Σq is derived as the quotient of total gating charge (necessarily obtained from high-expression oocytes) divided by the number of conducting channels as obtained, e.g., from fluctuation analysis of ionic currents. Again we want to emphasize that a constant ratio of charge over conductance as found, e.g., in the study of Schoppa et al. (1992) for K^+ channels suggests fully functional channels in contrast to the variable ratio in our study.

In conclusion, we found in whole oocyte experiments with high expression of sodium channels a low and variable percentage of ion-conducting channels compared to gating-current-producing channels. The ratio showed a clear inverse correlation to the internal sodium concentration or, rather, the influx of sodium ions. With respect to the underlying cause for the low sodium permeability or probably large fraction of silent sodium channels we speculate as follows. The sodium load represents an energetic stress if the cell tries to actively pump out the surplus of sodium. The fact that the influx either due to leak or pulsed I_{Na} would cause more change of cytoplasmic free sodium than actually observed strongly suggests an enforced activity of Na/K-ATP-ase for sodium homeostasis consuming, thereby, ~1 mM/l/min ATP. One could well imagine that this modulates directly or indirectly the conductivity of the sodium channels. Interestingly, for the structurally different amiloride-sensitive sodium channel ENaC expressed in *Xenopus* oocytes, a down-regulation of its conductance for Na^+ is convincingly shown to depend on $[Na^+]_i$ or Na^+ influx (see, e.g., Garty and Palmer, 1997; Kellenberger et al., 1998). This down-regulation seems not to be mediated by cytosolic Ca^{2+}, but there is evidence for an involvement of G-proteins (Komwatana et al., 1996). Besides a short-term down-regulation there is also a long-term effect in that incubation of cRNA-injected oocytes in low Na^+ solutions

allows a higher expression of ENaC at the cell surface, while sodium influx reduces it. We also had evidence for a long-term effect for the rBIIA channels. Assuming a continuous stress of the oocytes during the time of incubation and channel expression using the high-expression vectors, we tried to protect the cells during incubation by adding 2 μM TTX to the incubation bath during the 2–15 days of channel expression in the incubator. Over a long period, we consistently made the observation that the oocytes became more stable in TTX incubation and seemed to express a higher number of channels more quickly. We did not study this in detail, but found further evidence in this direction in ongoing studies on mutated channels (Kühn and Greeff, in preparation; Kühn and Greeff, 2000). The TTX-resistant mutant D384N, which has only a negligible conductance for sodium (Pusch et al., 1991) gave comparably large gating currents. In contrast, channels with handicapped inactivation and being leaky for sodium, such as the mutants of rBIIA IFM/QQQ or the *Paramyotonia congenita* equivalent R1626C, gave much less gating current and only relatively small ionic currents. The oocytes expressing these mutants also showed more positive resting potentials (-10 to $+20$ mV instead of the typical -20 to -40 mV), which indicated an influence of open sodium channels at rest. All these observations support the interpretation that a continuous sodium load impairs the expression of channels. The down-regulation of sodium permeability under the enhanced sodium influx observed in our experiments, therefore, could well be the consequence of an enhanced energy consumption needed to regulate the Na^+ concentration. It remains open how the channels are affected, but it seems rather likely that a change in the ATP/ADP ratio could cause a change in the phosphorylation state of a mediator or of the channels directly, such that they are not able to conduct ions but still have their voltage sensors producing gating current.

We thank Dr. Alan L. Goldin (Irvine, CA) for providing cDNA of the wild-type rat brain IIA sodium channel (pVA2580), the high expression vector and for valuable advice and discussions; further thanks go to Dr. Ligia Toro for providing the Shaker potassium clone and advice on high expression cRNA. We would like to thank H.R. Polder (npi-electronics, Tamm, Germany) for the efficient collaboration in the optimization of the voltage clamp. Our thanks go also to W. Kathe for his help in the initial stage of this study.

The work was supported by the Swiss National Science Foundation (31-37987.93) and the Hartmann-Müller-Stiftung.

REFERENCES

Aggarwal, S. K., and R. MacKinnon. 1996. Contribution of the S4 segment to gating charge in the *Shaker* K^+ channel. *Neuron.* 16:1169–1177.

Almers, W. 1978. Gating currents and charge movements in excitable membranes. *Rev. Physiol. Biochem. Pharmacol.* 82:96–190.

Armstrong, C. M. 1981. Sodium channels and gating currents. *Physiol. Rev.* 61:644–683.

Armstrong, C. M., and F. Bezanilla. 1973. Currents related to movement of the gating particles of the sodium channels. *Nature.* 242:459–461.

Armstrong, C. M., and F. Bezanilla. 1977. Inactivation of the sodium channel. II. Gating current experiments. *J. Gen. Physiol.* 70:567–590.

Armstrong, C. M., and B. Hille. 1998. Voltage-gated ion channels and electrical excitability. *Neuron.* 20:371–380.

Auld, V. J., A. L. Goldin, D. S. Krafte, J. Marshall, J. M. Dunn, W. A. Catterall, H. A. Lester, N. Davidson, and R. J. Dunn. 1988. A rat brain Na^+ channel alpha subunit with novel gating properties. *Neuron.* 1:449–461.

Bangalore, R., G. Mehrke, K. Gingrich, F. Hofmann, and R. S. Kass. 1996. Influence of L-type Ca channel alpha 2/delta-subunit on ionic and gating current in transiently transfected HEK 293 cells. *Am. J. Physiol. Heart Circ. Physiol.* 270:H1521–H1528.

Baumgartner, W., L. Islas, and F. J. Sigworth. 1999. Two-microelectrode voltage clamp of *Xenopus* oocytes: voltage errors and compensation for local current flow. *Biophys. J.* 77:1980–1991.

Bekkers, J. M., I. C. Forster, and N. G. Greeff. 1990. Gating current associated with inactivated states of the squid axon sodium channel. *Proc. Natl. Acad. Sci. USA.* 87:8311–8315.

Bekkers, J. M., N. G. Greeff, and R. D. Keynes. 1986. The conductance and density of sodium channels in the cut-open squid giant axon. *J. Physiol. (Lond.).* 377:463–486.

Bekkers, J. M., N. G. Greeff, R. D. Keynes, and B. Neumcke. 1984. The effect of local anaesthetics on the components of the asymmetry current in the squid giant axon. *J. Physiol. (Lond.).* 352:653–668.

Bezanilla, F., E. Perozo, and E. Stefani. 1994. Gating of *Shaker* K^+ channels. II. The components of gating currents and a model of channel activation. *Biophys. J.* 66:1011–1021.

Bezanilla, F., and E. Stefani. 1998. Gating currents. *Methods Enzymol.* 293:331–352.

Bulatko, A. K., and N. G. Greeff. 1995. Functional availability of sodium channels modulated by cytosolic free Ca^{2+} in cultured mammalian neurons. *J. Physiol. (Lond.).* 484:307–312.

Cha, A., P. C. Ruben, A. L. George, Jr., E. Fujimoto, and F. Bezanilla. 1999. Voltage sensors in domains III and IV, but not I and II are immobilized by Na^+ channel fast inactivation. *Neuron.* 22:73–87.

Chahine, M., A. L. George, Jr., M. Zhou, S. Ji, W. Sun, R. L. Barchi, and R. Horn. 1994. Sodium channel mutations in *Paramyotonia congenita* uncouple inactivation from activation. *Neuron.* 12:281–294.

Chen, L.-Q., V. Santarelli, R. Horn, and R. G. Kallen. 1996. A unique role for the S4 segment of domain 4 in the inactivation of sodium channels. *J. Gen. Physiol.* 108:549–556.

Chiamvimonvat, N., M. T. Perez-Garcia, G. F. Tomaselli, and E. Marban. 1996. Control of ion flux and selectivity by negatively charged residues in the outer mouth of rat sodium channels. *J. Physiol. (Lond.).* 491: 51–59.

Conti, F., L. J. DeFelice, and E. Wanke. 1975. Potassium and sodium ion current noise in the membrane of the squid giant axon. *J. Physiol. (Lond.).* 248:45–82.

Conti, F., A. Gheri, M. Pusch, and O. Moran. 1996. Use dependence of tetrodotoxin block of sodium channels: a revival of the trapped-ion mechanism. *Biophys. J.* 71:1295–1312.

Conti, F., and W. Stühmer. 1989. Quantal charge redistributions accompanying the structural transitions of sodium channels. *Eur. Biophys. J.* 17:53–59.

Dick, D. A., and D. J. Fry. 1975. Sodium fluxes in single amphibian oocytes: further studies and a new model. *J. Physiol. (Lond.).* 247: 91–116.

Forster, I. C., and N. G. Greeff. 1990. High resolution recording of asymmetry currents from the squid giant axon: technical aspects of voltage clamp design. *J. Neurosci. Meth.* 33:185–205.

Galili, G., E. E. Kawata, L. D. Smith, and B. A. Larkins. 1988. Role of the 3′-poly(A) sequence in translational regulation of mRNAs in *Xenopus laevis* oocytes. *J. Biol. Chem.* 263:5764–5770.

Garty, H., and L. G. Palmer. 1997. Epithelial sodium channels: function, structure, and regulation. *Physiol. Rev.* 77:359–396.

Goldin, A. L. 1991. Expression of ion channels by injection of mRNA into *Xenopus* oocytes. *Methods Cell Biol.* 36:487–509.

Greeff, N. G., and I. C. Forster. 1991. The quantal gating charge of sodium channel inactivation. *Eur. Biophys. J.* 20:165–176.

Greeff, N. G., R. D. Keynes, and D. F. Van Helden. 1982. Fractionation of the asymmetry current in the squid giant axon into inactivating and non-inactivating components. *Proc. R. Soc. (Lond.). B.* 215:375–389.

Greeff, N. G., and F. J. P. Kühn. 2000. Sodium load of *Xenopus* oocytes during high expression of rBIIA sodium channels reduces the ratio of ion permeability to gating charge. *Biophys. J.* 78:84*a*. (Abstr.).

Greeff, N. G., F. J. P. Kühn, and W. Kathe. 1998. Gating currents reveal hidden rat IIA sodium channel expression in *Xenopus* oocytes. *Biophys. J.* 74:148 *a*. (Abstr.).

Greeff, N. G., and H. R. Polder. 1998. Optimization of a two-electrode voltage clamp for recording of sodium ionic and gating currents from *Xenopus* oocytes. *Biophys. J.* 74:402 *a*. (Abstr.).

Hille, B. 1975. Ionic selectivity, saturation and block in sodium channels. A four barrier model. *J. Gen. Physiol.* 66:535–560.

Hille, B. 1992. Ionic Channels of Excitable Membranes, 2nd Ed. Sinauer Assoc. Inc., Sunderland, MA.

Hirschberg, B., A. Rovner, M. Liebermann, and J. Patlak. 1995. Transfer of twelve charges is needed to open skeletal muscle Na^+ channels. *J. Gen. Physiol.* 106:1053–1068.

Hodgkin, A. L., and A. F. Huxley. 1952. A quantitative description of membrane current and its application to conduction and excitation in nerve. *J. Physiol. (Lond.).* 117:500–544.

Horn, R. 1996. Counting charges [comment]. *J. Gen. Physiol.* 108: 129–132.

Horowitz, P., and W. Hill. 1980. The Art of Electronics. Cambridge University Press, Cambridge.

Horowitz, S. B., and P. L. Paine. 1979. Reference phase analysis of free and bound intracellular solutes. I. Sodium and potassium in amphibian oocytes. *Biophys. J.* 25:33–44.

Ji, S., A. L. George, Jr., R. Horn, and R. L. Barchi. 1996. *Paramyotonia congenita* mutations reveal different roles for segments S3 and S4 of domain D4 in hSkM1 sodium channel gating. *J. Gen. Physiol.* 107: 183–194.

Jones, L. P., C. D. DeMaria, and D. T. Yue. 1999. N-type calcium channel inactivation probed by gating-current analysis. *Biophys. J.* 76: 2530–2552.

Jones, L. P., S. K. Wie, and D. T. Yue. 1998. Mechanism of auxiliary subunit modulation of neuronal alpha1E calcium channels. *J. Gen. Physiol.* 112:125–143.

Josephson, I. R., and G. Varadi. 1996. The beta subunit increases Ca^{2+} currents and gating charge movements of human cardiac L-type Ca^{2+} channels. *Biophys. J.* 70:1285–1293.

Kamp, T. J., M. T. Perez-Garcia, and E. Marban. 1996. Enhancement of ionic current and charge movement by coexpression of calcium channel beta 1A subunit with alpha 1C subunit in a human embryonic kidney cell line. *J. Physiol. (Lond.).* 492:89–96.

Kellenberger, S., I. Gautschi, B. C. Rossier, and L. Schild. 1998. Mutations causing Liddle Syndrome reduce sodium-dependent downregulation of the epithelial sodium channel in the *Xenopus* oocyte expression system. *J. Clin. Invest.* 101:2741–2750.

Keynes, R. D., and E. Rojas. 1974. Kinetics and steady-state properties of the charged system controlling sodium conductance in the squid giant axon. *J. Physiol. (Lond.).* 239:393–434.

Komwatana, P., A. Dinudom, J. A. Young, and D. I. Cook. 1996. Cytosolic Na^+ controls an epithelial Na^+ channel via the G_o guanine nucleotide binding regulatory protein. *Proc. Natl. Acad. Sci. U.S.A.* 93:8107–8111.

Kontis, K. J., and A. Goldin. 1997. Sodium channel inactivation is altered by substitution of voltage sensor positive charges. *J. Gen. Physiol.* 110:403–413.

Kühn, F. J. P., and N. G. Greeff. 1999. Movement of voltage sensor S4 in domain 4 is tightly coupled to sodium channel fast inactivation and gating charge immobilization. *J. Gen. Physiol.* 114:167–183.

Kühn, F. J. P., and N. G. Greeff. 2000. Mutation of the selectivity filter domain alters recovery and immobilization of gating charge in rBIIA Na^+ channels. *Biophys. J.* 78:83*a*. (Abstr.).

Marban, E., T. Yamagishi, and G. F. Tomaselli. 1998. Structure and function of voltage-gated sodium channels. *J. Physiol. (Lond.)* 508: 647–657.

Neely, A., X. Wie, R. Olcese, L. Birnbaumer, and E. Stefani. 1993. Potentiation by the beta subunit of the ratio of the ionic current to the charge movement in the cardiac calcium channel. *Science.* 262:575–578.

Patton, D. E., and A. L. Goldin. 1991. A voltage-dependent gating transition induces use-dependent block by tetrodotoxin of rat IIA sodium channels expressed in *Xenopus* oocytes. *Neuron.* 7:637–647.

Patton, D. E., J. W. West, W. A. Catterall, and A. L. Goldin. 1992. Amino acid residues required for fast sodium channel inactivation, charge neutralizations and deletions in the III-IV linker. *Proc. Natl. Acad. Sci. U.S.A.* 89:10905–10909.

Perozo, E., R. MacKinnon, F. Bezanilla, and E. Stefani. 1993. Gating currents from a non-conducting mutant reveal open-closed conformations in *Shaker* K^+ channels. *Neuron.* 11:353–358.

Perozo, E., L. Santacruz-Toloza, E. Stefani, F. Bezanilla, and D. M. Papazian. 1994. S4 mutations alter gating currents of *Shaker* K^+ channels. *Biophys. J.* 66:345–354.

Pusch, M. 1990. Open-channel block of Na^+ channels by intracellular Mg^{2+}. *Eur. Biophys. J.* 18:317–326.

Pusch, M., F. Conti, and W. Stühmer. 1989. Intracellular magnesium blocks sodium outward currents in a voltage- and dose-dependent manner. *Biophys. J.* 55:1267–1271.

Pusch, M., M. Noda, W. Stühmer, S. Numa, and F. Conti. 1991. Single point mutations of the sodium channel drastically reduce the pore permeability without preventing its gating. *Eur. Biophys. J.* 20:127–133.

Richter, J. D., and L. D. Smith. 1981. Differential capacity for translation and lack of competition between mRNAs that segregate to free and membrane-bound polysomes. *Cell.* 27:183–191.

Ruben, P. C., A. Fleig, D. Featherstone, J. G. Starkus, and M. D. Rayner. 1997. Effects of clamp rise-time on rat brain IIA sodium channels in *Xenopus* oocytes. *J. Neurosci. Meth.* 73:113–122.

Schoppa, N. E., K. McCormack, M. A. Tanouye, and F. J. Sigworth. 1992. The size of gating charge in wild-type and mutant *Shaker* potassium channels. *Science.* 255:1712–1715.

Schreibmayer, W., H. A. Lester, and N. Dascal. 1994. Voltage clamping of *Xenopus laevis* oocytes utilizing agarose-cushion electrodes. *Pflügers Arch.* 426:453–458.

Shih, T. M., R. D. Smith, L. Toro, and A. L. Goldin. 1998. High-level expression and detection of ion channels in *Xenopus* oocytes. *Methods Enzymol.* 293:529–556.

Sigg, D., and F. Bezanilla. 1997. Total charge movement per channel: the relation between gating charge displacement and the voltage sensitivity of activation. *J. Gen. Physiol.* 109:27–39.

Sigworth, F. J. 1980. The variance of sodium current fluctuations at the node of Ranvier. *J. Physiol. (Lond.).* 307:97–129.

Sigworth, F. J. 1994. Voltage gating of ion channels. *Q. Rev. Biophys.* 27:1–40.

Sigworth, F. J. 1995. Charge movement in the sodium channel. *J. Gen. Physiol.* 106:1047–1051.

Stefani, E., and F. Bezanilla. 1998. Cut-open oocyte voltage-clamp technique. *Methods Enzymol.* 293:300–318.

Stefani, E., L. Toro, E. Perozo, and F. Bezanilla. 1994. Gating of *Shaker* K^+ channels. I. Ionic and gating currents. *Biophys. J.* 66:996–1010.

Stühmer, W., F. Conti, H. Suzuki, X. Wang, M. Noda, N. Yahagi, H. Kubo, and S. Numa. 1989. Structural parts involved in activation and inactivation of the sodium channel. *Nature.* 339:597–603.

Vassilev, P. M., T. Scheuer, and W. A. Catterall. 1988. Identification of an intracellular peptide segment involved in sodium channel inactivation. *Science.* 241:1658–1661.

Yang, N., A. L. George, Jr., and R. Horn. 1996. Molecular basis of charge movement in voltage-gated sodium channels. *Neuron.* 16:113–122.

Yang, N., and R. Horn. 1995. Evidence for voltage dependent S4 movements in sodium channels. *Neuron.* 15:213–218.